Thermo-tectonic evolution of a convergent orogen with low topographic build-up

Merten, S.

2011

document version
Publisher's PDF, also known as Version of record

CHAPTER 2

Low-temperature thermochronology

2.1 Introduction

Thermochronology is a technique that can be used to constrain the thermal history of rock samples or regions [e.g. *Reiners et al.*, 2005; *Braun et al.*, 2006]. The principle of thermochronology is based on the interplay between the accumulation of radioactive decay products in minerals (a radiogenic isotope or a crystallographic feature), and the thermally activated removal of that daughter product [e.g. *Braun et al.*, 2006]. Each radiometric dating method based on this principle is sensitive to a specific temperature, generally referred to as the "closure temperature" [*Dodson*, 1973]. Because temperature increases with depth in the Earth's lithosphere, temperature can be converted to estimated depth by assuming a geothermal gradient. Thermochronological data can thus provide insights on the subsurface depth at which rocks resided at a given time [e.g. *Braun et al.*, 2006].

Thermochronometers cover a wide temperature range from ∼900°C for the zircon (U-Th)/Pb) method [*Cherniak and Watson*, 2001] to ∼75°C for the apatite (U-Th)/He method [*Wolf et al.*, 1996] (Figure 2.1). The interest in earth-surface processes and interactions between tectonics, erosion and climate has drawn the attention to techniques that can provide constraints on near-surface time-temperature (t-T) histories of rocks (i.e. below temperatures of ∼300°C; Figure 2.1) [e.g. *Reiners et al.*, 2005]. The apatite fission track (AFT) and apatite (U-Th)/He (AHe) thermochronometers are such techniques with closure temperatures of ∼110 ± 10°C [*Gleadow and Duddy*, 1981] and ∼75 ± 5°C [*Wolf et al.*, 1996], respectively. The closure temperatures for the fission track and (U-Th)/He thermochronometers only serve as an indication for the "retentivity" of each system, since they vary within that system as a function of grain size, chemical composition, and cooling rate [e.g. *Braun et al.*, 2006]. The transition from open-

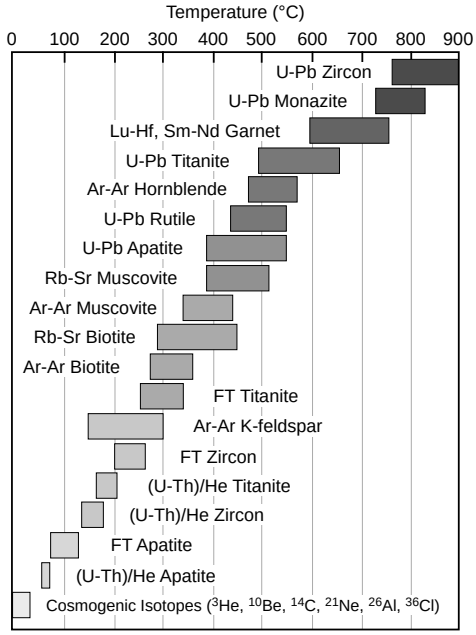

Figure 2.1: Diagram showing the mineral closure temperatures of isotopic methods used to reveal thermal histories of minerals and rocks [after http://su-thermochronology.syr.edu].

to closed-system behaviour is not instantaneous, but occurs over a discrete temperature interval, which is ∼120 to 60°C for the AFT method [e.g. *Gleadow and Duddy*, 1981] and ∼85 to 40°C for the AHe method [*Wolf et al.*, 1998]. Thus, for these methods the closure temperature concept is only applicable in the case of monotonic and rapid cooling through the temperature sensitivity window. In the case of complex cooling histories (e.g. reheating by burial or local intrusions), the closure temperatures have little to no significance, since the response of the AFT and AHe systems is a function of both the duration and magnitude of the heating event [e.g. *Reiners et al.*, 2005].

The AFT and AHe methods are commonly used to constrain the timing, amounts and rates of exhumation associated with mountain building, crustal deformation, extensional tectonics and landscape evolution [e.g. *Brown et al.*, 1994; *Gallagher et al.*, 1998; *Farley*, 2002; *Ehlers and Farley*, 2003; *Stockli*, 2005; *Reiners and Brandon*, 2006; *Lisker et al.*, 2009; *Olivetti et al.*, 2010; *Van der Beek et al.*, 2010]. In this study, AFT and AHe thermochronology have been combined to derive the late-stage evolution of the Romanian Carpathian orogen. Integrating multiple thermochronometers on the same sample suites allows for determinations of robust t-T histories and increases the confidence in the interpretation of the data sets [e.g. *Stockli et al.*, 2000; 2003; *Armstrong et al.*, 2003; *Reiners et al.*, 2003; *Balestrieri et al.*, 2005; *Danišík et al.*, 2010].

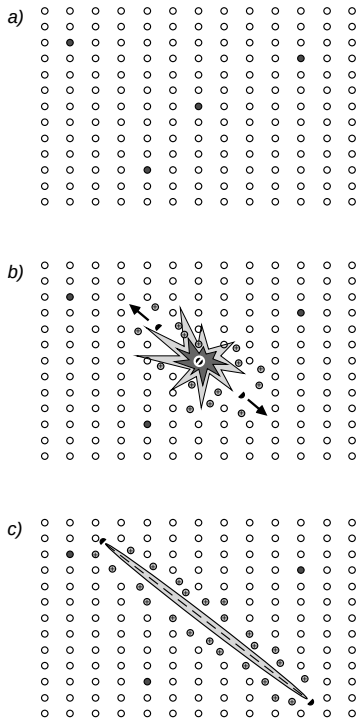

Figure 2.2: Cartoon representation of the ion spike explosion model and the formation of fission tracks in a mineral [modified after *Gallagher et al.*, 1998; *Hendriks*, 2003]. a) Trace amounts of radioactive ^{238}U are present in the crustal lattice (dark circles). b) Spontaneous fission of ^{238}U produces two highly charged heavy particles, which recoil as a result of Coulomb repulsion and interact with other atoms in the lattice initially by electron stripping or ionization. This leads to further deformation of the lattice as the ionized lattice atoms repel each other. c) As the fission particles capture electrons, they slow down and begin to interact by atomic collisions, further reducing the particles' energy until they come to rest, leaving a damage trail or fission track.

2.2 Apatite fission track (AFT) thermochronology

2.2.1 Fission track formation

Fission tracks are linear damage trails in the crystal lattice and form when highly charged nuclear particles travel through insulating solids during radioactive decay [e.g. *Wagner*, 1968]. In geological samples, natural or spontaneous tracks are produced nearly exclusively by spontaneous fission of ^{238}U, since other naturally occurring heavy isotopes (e.g. ^{232}Th and ^{235}U) have such long fission half-lives that they do not form a significant source for spontaneous track formation [e.g. *Wagner and Van den Haute*, 1992]. The preferred basic model for fission track formation is the ion spike explosion model [*Fleischer et al.*, 1965; 1975], which postulates that ^{238}U splits in two highly charged nuclear fragments travelling through the host mineral in a random but opposite direction creating linear zones of damage by ionisation of atoms in the crystal lattice (Figure 2.2). The ion spike explosion model should however be regarded as a first approximation of the track-forming process, because the physical processes involved are still under research [e.g. *Chadderton*, 1988; *Chadderton*, 2003; *Rabone et al.*, 2008].

Depending on the density of the crystal lattice, newly formed tracks in natural samples typically have lengths of 10–20 μm and widths of 25–50 Ångstroms, [*Wagner and Van den Haute*, 1992]. Because of these narrow widths, fission tracks are only visible using transmission electron microscopy [*Silk and Barnes*, 1959]. However, tracks can be enlarged by selectively dissolving the damage zones using a chemical etchant, which enables observation of the tracks using an optical

microscope [*Young*, 1958; *Price and Walker*, 1962]. Fission track analysis provides a practical method of dating minerals, given that each spontaneous fission event creates one fission track, the fission process occurs at a statistically constant rate and tracks can be observed optically after etching. It has become an important and successful tool in deciphering a variety of geological problems, including structural evolution of orogenic belts, sedimentary provenance, thermal history modelling of sedimentary basins, and long-term continental denudation [e.g. *Brown et al.*, 1994; *Gallagher et al.*, 1998]. Reviews of the technique can be found in e.g. *Wagner and Van den Haute* [1992], *Gleadow et al.* [2002], *Donelick et al.* [2005], and *Tagami and O'Sullivan* [2005].

In order to be useful as a dating method, the concentration of ^{238}U needs to be sufficient to produce a detectable number of fission events over geological time. This is the case for common minerals such as apatite, zircon and titanite, but also micas, volcanic glass and low-uranium epidotes and garnets can be useful [*Gleadow et al.*, 2002]. In this study, only apatite has been used for fission track dating. Apatite ($Ca_5(PO_4)_3$(F,Cl,OH)), was one of the first minerals to be investigated for fission track dating [*Fleischer and Price*, 1964]. It has become the most important mineral used for this dating method due to its tendency to concentrate uranium within its structure at the time of crystallisation and its widespread occurrence in all of the major rock groups (apart from limestones) [e.g. *Gleadow et al.*, 2002].

2.2.2 Age determination and calculation

A fission track age is given by the relative abundance of the parent and daughter product in the host mineral (i.e. the ^{238}U concentration and the spontaneous fission track density), and the decay constant for the parent nuclide. The fission track age equation is thus given by:

$$Age = \frac{1}{\lambda_D} ln \left(1 + \frac{\lambda_D}{\lambda_F} \frac{N_s}{^{238}U} \right) \tag{2.1}$$

where λ_D is the total decay constant of ^{238}U, which is very close to that for α-decay [1.55125×10^{-10} yr^{-1}; *Steiger and Jäger*, 1977], λ_F is the decay constant for spontaneous fission of ^{238}U [between 7.03×10^{-17} yr^{-1} to 8.46×10^{-17} yr^{-1}; *Wagner and Van den Haute*, 1992], N_s is the number of spontaneous fission tracks in the sample and ^{238}U is the number of ^{238}U atoms in the sample.

The number of spontaneous tracks can be counted directly on a polished and etched surface using an optical microscope. In order to derive the ^{238}U parent content, the most commonly used technique is the external detector method (EDM) [*Gleadow*, 1981; *Hurford and Green*, 1982], but procedures using laser ablation–inductively coupled plasma-mass spectrometry (LA–ICP-MS) to measure the uranium content for AFT dating are also under development [see *Hasebe et al.*, 2004; 2009; *Donelick et al.*, 2005 for further details]. In this study the EDM method was used (Figure 2.3), in which a thermally annealed U-free piece of mica is sealed against the polished and etched surface of the fission track mount and sent to a nuclear reactor. Irradiation of the samples with low-energy thermal neutrons induces fission of ^{235}U and some heavy particles will cross the interface between the mineral and the mica, producing a mirror image of the original

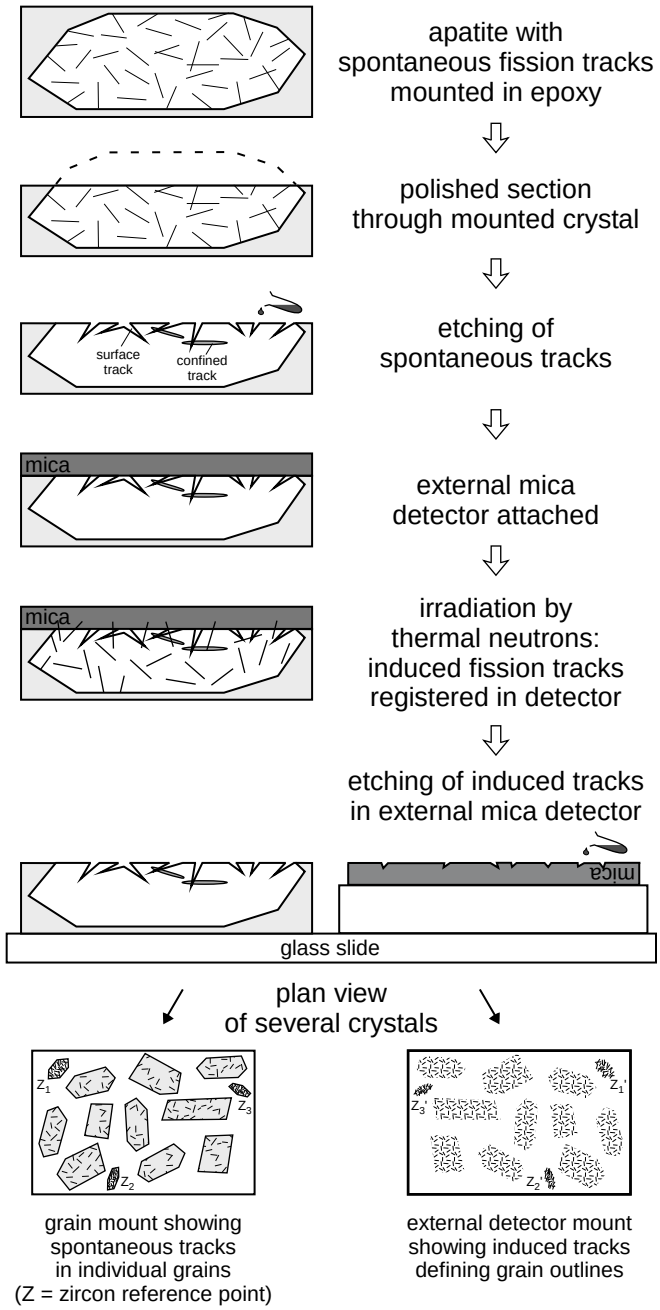

Figure 2.3: Schematic representation of the External Detector Method [modified after *Gallagher et al.*, 1998; *Hendriks*, 2003].

grain. After irradiation, the mica is etched to reveal the induced tracks. Since the $^{235}U/^{238}U$ ratio is constant in nature and the number of induced tracks is indicative for the amount of ^{235}U atoms present, the ^{238}U parent distribution can be determined. The major advantage of this method is that the same area is used to determine the density of spontaneous and induced tracks, and thus single grain ages can be obtained. A fission track age can then be calculated as follows [*Price and Walker*, 1963; *Naeser*, 1979]:

$$Age = \frac{1}{\lambda_D} ln \left(1 + \frac{\lambda_D}{\lambda_F} \frac{\rho_s}{\rho_i} I \sigma_F \Phi g \right) \tag{2.2}$$

where ρ_s is the spontaneous track density from ^{238}U (tracks/cm^2), ρ_i is the neutron-induced track density from ^{235}U (tracks/cm^2), I is the isotopic ratio $^{235}U/^{238}U$ (7.252×10^{-3}), σ_F is the cross-section for thermal neutron-induced fission of ^{235}U (584.25×10^{-24} cm^2), Φ is the thermal neutron fluence (neutrons/cm^2) and g is the geometry factor [0.5 for EDM; *Wagner and Van den Haute*, 1992].

In equation (2.2), the exact value of λ_F is not well determined [*Bigazzi*, 1981; Van den Haute et al., 1998], whereas it is generally difficult to measure Φ accurately [*Hurford and Green*, 1982; 1983]. This can be circumvented using the ζ ("Zeta") calibration method, in which the fission track age is calibrated against one or more mineral age standards [*Fleischer et al.*, 1975; *Hurford and Green*, 1982; 1983]. Φ can be determined by measuring the induced track density on a U-bearing standard glass monitor (ρ_d) irradiated together with the samples, and is given by:

$$\Phi = B \rho_d \tag{2.3}$$

where B is a calibration constant empirically determined. The constants in the equation can then be taken together in the ζ factor:

$$\zeta = \frac{\sigma_F I B}{\lambda_F} \tag{2.4}$$

Equation (2.2) can then be written as:

$$Age = \frac{1}{\lambda_D} ln \left(1 + \lambda_D \zeta \frac{\rho_s}{\rho_i} \rho_d g \right) \tag{2.5}$$

Because the ζ value was shown to vary for different minerals and different fission track researchers, standards with a calibrated age are irradiated with standard dosimeter glasses and analysed repeatedly to obtain a personal ζ calibration factor for a specific dosimeter [*Hurford and Green*, 1983]. The ζ value can then be calculated by rewriting equation (2.5):

$$\zeta = \frac{e^{\lambda_D t_{std}} - 1}{\lambda_D \left(\frac{\rho_s}{\rho_i} \right)_{std} \rho_d g} \tag{2.6}$$

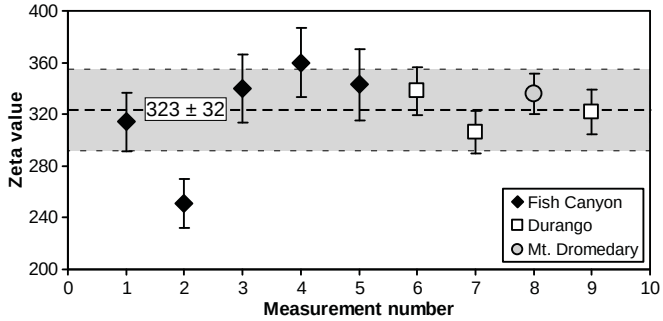

Figure 2.4: ζ values determined during this study by analyst S. Merten on Durango, Fish Canyon and Mount Dromedary apatites using CN-5 dosimeter standard glass.

where t_{std} is the reference age of the standard and $(\rho_s/\rho_i)_{std}$ is the ratio between the spontaneous and the induced track densities measured on the standard.

In this study, three apatite standards were used for ζ calibration for apatite and dosimeter glass CN5: Fish Canyon [27.9 ± 0.7 Ma; *Hurford and Green*, 1983], Durango [31.4 ± 0.5 Ma; *Green*, 1985] and Mt. Dromedary [98.7 ± 0.6 Ma; *Green*, 1985]. For all samples in this study, AFT age determinations were calculated using a ζ value of 323 ± 32 (Figure 2.4).

2.2.3 Stability and fading of tracks

Fission tracks are unstable and will tend to be repaired by solid-state diffusion processes, which is called annealing. As a result of annealing, the etchable length of the individual tracks, which is initially similar for all newly formed tracks in a given mineral structure (∼16 μm for apatite), is progressively shortened [*Green et al.*, 1986]. Because the proportion of tracks intersecting the polished surface of a grain is directly related to the track length, the progressive length reduction will also cause a decrease in fission track density and thus in fission track age [*Nagpaul et al.*, 1974; *Green*, 1988]. To quantify the effect of annealing, the distribution of track lengths, which can be obtained by measuring a sufficient number of tracks (preferably >100), also needs to be taken into account in order to derive the geological history recorded by the host mineral [*Gleadow et al.*, 1986].

Fission track annealing is a complex, non-linear process, of which the physics are still not fully understood. The annealing behaviour of fission tracks in apatite has been estimated by extrapolation of laboratory annealing data to geological time, showing that temperature and time are the main factors controlling annealing [*Fleischer et al.*, 1965; 1975; *Wagner*, 1968; *Naeser and Faul*, 1969; *Nagpaul et al.*, 1974]. The same pattern of thermal annealing of fission tracks at increased temperatures over geological time-scales was confirmed by deep borehole data [e.g. *Naeser and Forbes*, 1976; *Gleadow and Duddy*, 1981; *Corrigan*, 1993; *Wagner et al.*, 1994]. On geological time-scales, fission tracks in apatite anneal completely at temperatures >110 ± 10°C [e.g. *Wagner*, 1968; *Naeser*, 1979; *Gleadow and Duddy*, 1981; *Gleadow et al.*, 1986; *Green et al.*, 1986]. Anneal-

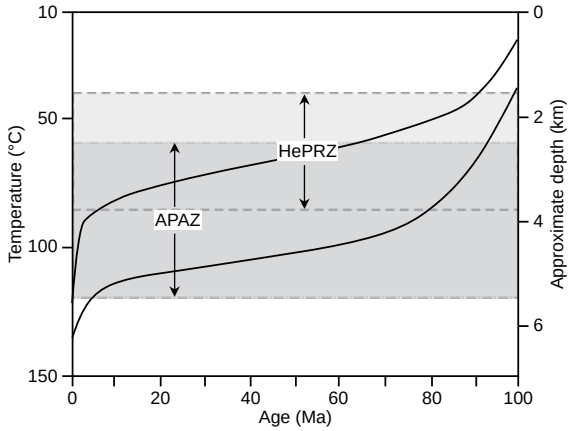

Figure 2.5: Apatite fission track Partial Annealing Zone (APAZ) and apatite Helium Partial Retention Zone (HePRZ), calculated assuming 100 Ma of isothermal holding at the temperatures indicated on the y-axis. The right-hand axis scales temperature into sub-crustal depth assuming a geothermal gradient of 20°C/km and a mean surface temperature of 10°C [modified after *Farley*, 2002; *Foeken*, 2004].

ing of produced fission tracks occurs at decreasing rates over geological time in the temperature range of ∼110–60°C, referred to as the apatite partial annealing zone or APAZ (Figure 2.5) [e.g. *Gleadow and Duddy*, 1981; *Naeser*, 1981]. Below ∼60°C, annealing rates are very low and the tracks are generally considered stable. However, mean track lengths (MTLs) for spontaneous tracks measured in natural samples considered to have cooled rapidly through the APAZ and to have remained near surface temperatures since their formation are between 14 and 15 μm, whereas artificially generated new fission tracks generally show etchable track lengths between 15.8 and 16.6 μm at room temperature [e.g. *Wagner and Storzer*, 1970; *Bertel et al.*, 1977; *Green*, 1980; *Gleadow et al.*, 1986]. This discrepancy of ∼1.0–1.5 μm between fossil and induced track lengths has been ascribed to low-temperature annealing [e.g. *Donelick et al.*, 1990; *Vrolijk et al.*, 1992]. *Spiegel et al.* [2007] have shown that exposure to temperatures between ∼10 and ∼70°C over geological time-scales (∼15–120 Ma) results in track shortening between 4 and 11% and that thus, even at very low temperatures the AFT system might not be acting as a fully closed system.

The orientation of the tracks with respect to the crystallographic c-axis is another factor that determines the annealing rate of fission tracks. Tracks at high angles to the apatites crystallographic c-axis are known to anneal faster than tracks at low angles [*Green et al.*, 1986; *Donelick*, 1991; *Crowley et al.*, 1991; *Donelick et al.*, 1999; *Barbarand et al.*, 2003a]. Because of this anisotropy, track lengths should be measured on polished surfaces parallel to the c-axis of the apatite crystal and on horizontal tracks that are completely contained within the host mineral, i.e., the so-called confined tracks [*Gleadow et al.*, 1986]. These confined tracks are etched from the intersection with another track (track-in-track, i.e. TINT) or a cleavage (track-in-cleavage, i.e. TINCLE) [*Lal et al.*, 1969]. If horizontal confined tracks would be measured in a basal section of annealed apatite,

all tracks will be perpendicular to the c-axis and therefore will be shorter than tracks in other orientations, introducing a severe bias to the measurements. In a prismatic section, however, horizontal confined tracks will be present in all orientations to the c-axis so that the anisotropy is incorporated into the measurements [*Green et al.*, 1986].

The chemical composition of the apatite crystal is also known to have a significant influence on the annealing properties, although its exact role remains poorly understood. Chlorine content seems to play a dominant role in that chlorine-rich apatites seem to be more resistant to track annealing than fluorine-rich apatites [*Gleadow and Duddy*, 1981; *Green et al.*, 1985; 1986; *Crowley et al.*, 1990; *O'Sullivan and Parrish*, 1995], but also substitutions with other elements may cause differences in annealing. These include Mn, Sr, Fe, rare earth elements (REE), OH, CO_3 and SiO_2 [*Ravenhurst et al.*, 1993; *Burtner et al.*, 1994; *Carpéna*, 1998; *Carlson et al.*, 1999; *Barbarand and Pagel*, 2001; *Barbarand et al.*, 2003b; *Spiegel et al.*, 2007].

Annealing behaviour can be correlated with the etching characteristics of the host apatite with the measurable D_{par} parameter, which is the c-axis parallel etch pit diameter intersecting a polished and etched apatite surface [*Donelick*, 1993; *Burtner et al.*, 1994; *Carlson et al.*, 1999; *Ketcham et al.*, 1999; *Barbarand et al.*, 2003b]. Since the revealed tracks and etch pits observed under the optical microscope are a result of the interaction between the mineral defects and the etching agent, the D_{par} size also depends on the etch conditions. For apatites etched according to the *Carlson et al.* [1999] procedure (20 ± 0.5 seconds in 5.5 M nitric acid at 21 ± 1°C), grains least resistant to annealing (i.e. D_{par} = 1.50 μm) appear to experience total fission-track annealing at around 100–110°C in the geological environment, whereas the ones most resistant to annealing (i.e. D_{par} = 3.00 μm) experience total fission-track annealing at temperatures greater than 160°C [*Ketcham et al.*, 1999]. The D_{par} is positively correlated with Cl wt% and OH wt% and negatively correlated with F wt%, in that small D_{par} values (<2 μm) are typical for fluorine-rich apatites, whereas larger values (2–5 μm) are characteristic for chlorine-rich apatites [*Burtner et al.*, 1994].

Other factors might add to the complexity of annealing behaviour of fission tracks in apatite. Based on laboratory experiments, which showed a strong decrease in annealing rate as a function of increasing pressure and an increase in fission track recovery as a function of stress, *Wendt et al.* [2002] suggested that annealing characteristics depend on confining pressure and stress. The evidence is however ambiguous and highly controversial [*Chadderton*, 2003; *Donelick et al.*, 2003; *Kohn et al.*, 2003; 2004; *Vidal et al.*, 2003; *Wendt et al.*, 2003].

Accumulated radiation damage due to the α-decay of trace U and Th potentially affects annealing kinetics [*Hendriks and Redfield*, 2005]. He-ion irradiation experiments on pre-damaged fluorapatites have demonstrated that α-particle emission can result in recovery of lattice defects, with the efficiency depending on dose rate and time [*Ouchani et al.*, 1997; *Soulet et al.*, 2001; *Chaumont et al.*, 2002]. *Miro et al.* [2005] confirmed this defect healing behaviour of apatite upon α-irradiation specifically for damage induced by fission fragments. Although α-annealing acts simultaneously with thermal annealing at elevated temperatures (>60°C), at lower temperatures α-annealing might be the dominant process of

recovery in fluorapatite over geological times [*Chaumont et al.*, 2002; *Hendriks and Redfield*, 2005]. However, the radiation enhanced annealing effect in apatite is still a matter of debate and further research in both geological and experimental settings is required [e.g. *Donelick et al.*, 2005; *Hendriks and Redfield*, 2005; 2006; *Larson et al.*, 2006; *Kohn et al.*, 2009].

2.2.4 Laboratory and analytical procedures

For this study, samples for AFT analysis were collected from two different areas in the Romanian Carpathians (Chapter 1, Figure 1.1): the Apuseni Mountains (Appendix A, Table A.1) and the SE Carpathians (Appendix A, Table A.2). Apatites were separated from whole rock samples (∼4 kg) with standard mineral separation procedures used at the VU University Amsterdam [e.g. *Murrell*, 2003; *Juez-Larré*, 2003; *Foeken*, 2004]. Since regular mineral separation procedures did not yield pure enough apatite selections for samples from the SE Carpathians, the 90–200 μm grain size range was handpicked to take out the non-apatites. For samples from the Apuseni Mountains, the <60 μm to 200 μm grain size range was used for AFT. Grains were mounted in epoxy resin and subsequently grinded and polished to reveal the apatites surface. Two mounts were prepared for each sample; one for age determinations and one for confined track length measurements.

Mounts for age determination were etched for 35 seconds (samples Apuseni Mountains; Table A.1) and 40 seconds (samples SE Carpathians; Table A.2) in 1.6 M nitric acid at 21°C to reveal clearly visible spontaneous tracks [*Murrell*, 2003; *Murrel et al.*, 2009]. Samples were dated by external detector method (EDM) with muscovite detectors [*Gleadow and Duddy*, 1981] and irradiated at the low-flux reactor of the ECN in Petten, the Netherlands. CN5 dosimeter glasses of known uranium content with external mica detectors [*Hurford and Green*, 1982; 1983; *Wagner and Van den Haute*, 1992] were included to determine the neutron flux during irradiation. After irradiation, the external mica detectors of samples and dosimeter glasses were etched in 48% hydrofluoric acid at 21°C for 12 and 25 minutes, respectively. Tracks in apatites and mica detectors were counted with an Olympus BX51 optical microscope with 500× magnification using dry objective. Positioning of the grain mount and mica mirror image was driven by the AUTOSCAN^{TM} Systems Pty Ltd computerized microscope stage. AFT ages were calculated using TRACKKEY (version 4.2.g) [*Dunkl*, 2002]. Statistical uncertainties on ages are quoted at the $\pm$ 1σ level.

Separate mounts were prepared for length measurements. Previous AFT studies of the Carpathians [*Sanders et al.*, 1999] showed that spontaneous fission track densities were too low to allow enough track length measurements. Thus TINT (tracks-in-track) fission track densities in length mounts were enhanced prior to etching, using ^{252}Cf-derived fission fragment tracks [*Donelick and Miller*, 1991]. Subsequently, length mounts were etched in 1.6 M nitric acid for 35 (Apuseni Mountains) and 40 (SE Carpathians) seconds at 21°C. Lengths of horizontal confined tracks, the angle between the track and c-axis of the crystal, and etch pit diameters (D_{par}) were measured with a magnification of 1000×. Confined track lengths are normalized for track angle using the c-axis projection model

of *Donelick et al.* [1999] to increase the consistency of the measurements and to compensate for Cf-irradiation and observer bias [e.g. *Barbarand et al.*, 2003a; *Ketcham*, 2005a; *Ketcham et al.*, 2007a; 2009]. Etch pit diameters (D_{par}) were measured on both age- and track length mounts in order to constrain the kinetic characteristics of the apatite grains [*Donelick*, 1993; *Burtner et al.*, 1994; *Ketcham et al.*, 1999].

2.2.5 Statistical analysis of single grain age data

To obtain an AFT age using the EDM method, multiple single grain ages are determined for each sample. It was aimed to count ∼20–30 grains for basement and magmatic rock samples and >40 grains for sedimentary rocks. Restricted by apatite quantity and quality, 4–38 grains per sample could be analysed for the Apuseni Mountains (Table A.1) and 21–80 grains for the SE Carpathians (Table A.2). The AFT sample age can subsequently be expressed as pooled, mean, and central age. The pooled age is simply determined by the sum of all the spontaneous counts divided by the sum of all the induced counts. This is only meaningful if all the individual grain ages belong to a single homogeneous population, which is not necessarily the case [e.g. *Galbraith and Green*, 1990; *Galbraith and Laslett*, 1993; *Brandon et al.*, 1998]. Single grain ages can be dispersed when grains come from multiple sources recording different pre-depositional t-T histories (i.e. in sediments), or when differential annealing occurs between grains with different compositions. The homogeneity of a sample can be assessed by the Chi-square (χ^2) test, which compares the observed variance within the population of grain ages with the variance predicted for the radioactive decay process alone [*Galbraith*, 1981; *Brandon*, 1992]. The test returns P(χ^2), the probability that the difference between observed and predicted variances could be due to random chance alone. When a sample returns a P(χ^2) value >5%, the age population can considered to be homogenous. For samples with a P(χ^2) value <5%, the individual grains cannot be considered to belong to a single age population. In the latter case, the mean age is calculated, which is the arithmetic mean of the individual ratios of spontaneous to induced tracks. Furthermore, the central age can be calculated, which is the mean of the logarithmic normal distribution of single grain ages weighted by the precision of the individual measurements [*Galbraith and Laslett*, 1993]. The age dispersion can then be assessed by the relative standard deviation of the population age [*Galbraith and Laslett*, 1993]. Dispersions <10% suggest minor variations between grain ages, whereas values >40% point to considerable heterogeneity. Note that the pooled, mean and central age estimates are essentially the same when the variation in the population is consistent with a Poisson distribution.

Inhomogeneous AFT age populations with P(χ^2) values <5% and dispersions >30% were obtained for most of the sediment samples from the SE Carpathians (Table A.2 and Chapter 4). The Binomfit program [developed by M. Brandon and summarized in *Ehlers et al.*, 2005] was used to identify different age components and to calculate population ages and uncertainties for these heterogeneous samples. The Binomfit algorithm is based on the binomial peak-fitting method of *Galbraith and Green* [1990]. It provides an iterative search of peak ages and

number of peaks to find an optimal solution. The quality of fit for each trial solution is scored using χ^2 statistics, in a manner similar to the conventional χ^2 test [*Brandon*, 2002].

2.3 Apatite (U-Th)/He (AHe) thermochronology

(U-Th)/He dating generally involves analysis of U and Th rich accessory minerals able to retain ^{4}He. There is a large family of minerals potentially suitable for (U-Th)/He thermochronology, but minerals most commonly used for (U-Th)/He dating are apatite, zircon and titanite. In this study, only apatite has been used.

2.3.1 ^{4}He ingrowth

^{4}He nuclei (α-particles) and several Pb isotopes are produced by the decay series of ^{232}Th, ^{235}U and ^{238}U (^{4}He production from ^{147}Sm decay occurs, but can generally considered to be negligible due to low or absent ^{147}Sm concentrations in apatite). Excluding ^{147}Sm, the ^{4}He ingrowth equation can be written as:

$$^4He = 8 \cdot {}^{238}U\left(e^{\lambda_{238}t} - 1\right) + 7 \cdot \left(\frac{^{238}U}{137.88}\right)\left(e^{\lambda_{235}t} - 1\right) + 6 \cdot {}^{232}Th\left(e^{\lambda_{232}t} - 1\right) \tag{2.7}$$

where ^{4}He, ^{238}U and ^{232}Th indicate the measured present-day abundances of these isotopes, t is the accumulation time or He age, λ is a radioactive decay constant ($\lambda_{238} = 1.55125 \times 10^{-10}$ yr^{-1}, $\lambda_{235} = 9.849 \times 10^{-10}$ yr^{-1}, $\lambda_{232} = 4.948 \times 10^{-11}$ yr^{-1}), and (1/137.88) is the present-day ^{235}U/^{238}U ratio [e.g. *Farley*, 2002]. The coefficients that precede the U and Th abundances correspond to the number of α-particles for a single decay of ^{238}U, ^{235}U and ^{232}Th. Equation (2.7) assumes secular equilibrium among all daughters in the decay chain. This condition is guaranteed for crystals formed more than ~350 kyr prior to the onset of He accumulation [*Farley*, 2002], and is valid for most applications.

There are several factors that can bias measured He ages towards erroneously older or younger ages (e.g. presence of mineral/fluid inclusions, U and Th parent zonation) [*Farley*, 2002]. Equation (2.7) assumes no initial ^{4}He in the crystal being dated, which generally is a valid assumption [*Farley*, 2002]. The presence of fluid inclusions carrying crustal or mantle ^{4}He may violate this assumption, and consequently will bias He ages towards older ages [*Lippolt et al.*, 1994; *Warnock et al.*, 1997; *Stockli et al.*, 2000].

The presence of small U-Th rich mineral inclusions is another factor that can bias the measured He age [e.g. *Lippolt et al.*, 1994; *House et al.*, 1997; *Warnock et al.*, 1997; *Stockli et al.*, 2000; *Farley*, 2002; *Ehlers and Farley*, 2003]. In apatite, the most common inclusions are zircon and monazite [*Farley and Stockli*, 2002], of which the size may vary from a few microns to a size almost equal to the apatite grain itself. The main problem with U-Th rich mineral inclusions is that they eject He into the apatite host crystal, which will be released upon mineral heating. If the inclusions are not completely dissolved during mineral dissolution (especially zircon is notoriously difficult to dissolve), some of the He will be "par-

entless" and results in erroneously old AHe ages [e.g. *House et al.*, 1997; *Warnock et al.*, 1997; *Farley*, 2002]. However, *Vermeesch et al.* [2007] showed that single U or Th rich inclusions less than a few percent of the volume of the host apatite are unlikely to contribute substantial radiogenic He. For larger inclusions or multiple small inclusions, the parentless helium problem can be partially solved by more aggressive acid dissolution procedures [*Vermeesch et al.*, 2007]. Microscopic examination of grains to be dated and subsequent removal of grains with inclusions greatly reduces the problem [*Farley*, 2002], but some inclusions remain extremely difficult to detect [*Farley*, 2002; *Ehlers and Farley*, 2003]. The re-extraction test and age irreproducibility of replicate measurements are good assessments to identify previously undetected inclusions in measured samples [e.g. *House et al.*, 1999; *Farley*, 2002; *Ehlers and Farley*, 2003].

Another factor that can strongly bias measured He ages stems from the fact that α-particles emitted during the U and Th series decay are emitted with high kinetic energies ($\sim$4–8 MeV). In this process, the α-particles require tens of microns to come to rest within solid matter, a distance known as the stopping distance [*Ziegler*, 1977]. The series averaged mean stopping distances for ^{238}U, ^{235}U and ^{232}Th in apatite were computed to be 19.68, 22.83 and 22.46 μm respectively, giving an average value of $\sim$20 μm for apatite [*Farley et al.*, 1996]. However, because of their indirect derivation, stopping distances for minerals are prone to revision as progress is made on various theoretical fronts [see *Ketcham*, 2009].

The effects of α-stopping distances on ^{4}He retention in a mineral are illustrated in Figure 2.6 and depend on the location of the parent nuclide within the crystal [*Farley*, 2002]. If the parent nuclide is located more than one stopping distance away from the crystal boundary, the α-particle will be retained in the crystal. If the parent nuclide lies within one stopping distance from the crystal boundary, the α-particle might be ejected from the mineral. The probability of ejection rises up to 50% when the parent nuclide is located along the grain edge. The probability of ^{4}He implantation is usually considered to be insignificant, because the contrast in parent element concentration between the apatite and the host rock is generally large [*Farley et al.*, 1996; *Farley*, 2002].

The loss of α-particles results in lower ^{4}He concentrations within the mineral than produced for the given parent element concentrations, and thus the measured AHe age will be too young [*Farley et al.*, 1996; *Farley*, 2002]. A quantitative model for correcting AHe ages for α-ejection loss has therefore been developed [*Farley et al.*, 1996]. For hexagonal prism geometry, the total amount of particles retained in the apatite crystal (F_T) is given by [*Farley et al.*, 1996]:

$$F_T = 1 + a_1\beta + a_2\beta^2 \; with \; \beta = \frac{(2.31L + 2R)}{RL} \tag{2.8}$$

where a_1 and a_2 are the fitting parameters incorporating the stopping distance and the density of the stopping medium (a_1 and a_2 are (-5.13) and (6.78) for the ^{238}U series, and (-5.9) and (8.99) for the ^{232}Th series), β is the surface to volume ratio of the crystal, and R and L are radius and length of the analysed crystal. In order to determine R and L, each apatite crystal used for AHe dating is photographed under a microscope, after which values for R and L are determined. Broken grains should be avoided, as they violate the assumed α-particle distribution

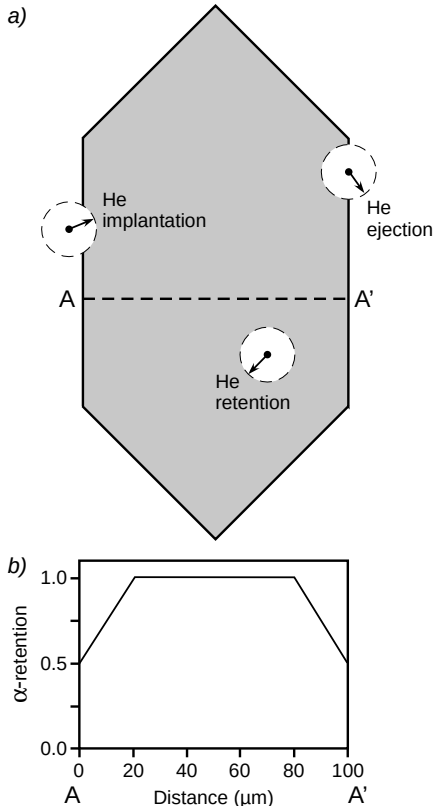

Figure 2.6: a) The effects of α-stopping distance on He retention in a mineral [after *Farley*, 2002]. The three shown scenarios within a schematic crystal are complete α-retention, possible α-ejection and possible α-implantation. b) Schematic cross-section showing how α-retention in an apatite crystal changes from rim to core to rim along path A–A' in Figure 2.6a [after *Farley*, 2002].

upon which the F_T correction is based. In order to quantify the error associated with the determination of R and L, repeated measurements of the radius and length are performed on each apatite. These measurements are subsequently averaged to obtain mean R and L values and errors are determined by using an error propagation calculation. F_T corrections in the range of ∼0.65 to ∼0.85 can typically be reproduced by individual observers to better than a few percent. At smaller grain sizes ($F_T < 0.65$), errors in F_T will increase rapidly [*Farley*, 2002].

To accommodate the slightly higher α-retentivity for ^{238}U than for ^{232}Th, a mean of the F_T values for U and Th is computed, using a weighting factor (a_{238}) [*Farley*, 2002]:

$$^{Mean}F_T = a_{238} \cdot {}^{238U}F_T + (1 - a_{238}) \cdot {}^{232Th}F_T \; with \; a_{238} = \frac{1}{\left(1.04 + 0.245\frac{Th}{U}\right)} \tag{2.9}$$

where Th/U is the measured Th/U ratio. The α-corrected AHe age is subsequently given by:

$$Corrected\ age = \frac{Measured\ age}{^{Mean}F_T} \tag{2.10}$$

In the case of rapid cooling, the α-correction model of *Farley et al.* [1996] and *Farley* [2002] is a good approximation to correct He ages. Due to some of the assumptions in the α-correction model, this procedure might, however, lead to errors for samples that resided at temperatures close to the closure temperature for prolonged periods [e.g. *Meesters and Dunai*, 2002a; 2002b]. The assumption of insignificant ^{4}He implantation, for example, may be violated in very U-Th poor apatites [e.g. *Farley*, 2002; *Spencer et al.*, 2004]. It has been shown that He implantation from surrounding host U-Th rich sedimentary components might lead to an overestimation of AHe ages up to 50% for apatites with low U content (<5 ppm) [*Spiegel et al.*, 2009]. Furthermore, the ejection model assumes homogeneous U and Th distribution [*Farley et al.*, 1996], which is generally not known prior to dating. The assumption of homogeneous U and Th distributions is often violated in natural apatites, due to zonation and/or the presence of U-Th rich mineral inclusions [*Farley et al.*, 1996; *Farley*, 2002; *Vermeesch et al.*, 2007]. If zoned crystals have a localisation of parent nuclides along the outer crystal rim, the parent-rich outer parts of the crystal will be strongly depleted in ^{4}He due to α-ejection. This will result in too young corrected ages [*Meesters and Dunai*, 2002b; *Hourigan et al.*, 2005]. Similarly, U-Th rich inclusions could result in erroneous α-ejection corrections. An inclusion that dominates the parent-element budget of the crystal (such as a zircon inclusion in apatite) would necessitate a $\sim$50% α-ejection loss correction if located at the surface of the host, and a 0% correction if the inclusion was sufficiently far from the surfaces of the host crystal to prevent any α-escape by recoil [e.g. *Boyce et al.*, 2009]. Furthermore, the assumption of linearity in the decay equation leads to α-correction errors for older samples (>500 Ma) [*Ketcham*, 2009].

2.3.2 ^{4}He diffusion

The measured AHe age is a combination of competing effects of radiogenic ^{4}He ingrowth from U and Th decay and the diffusive loss sustained during prolonged exposure to elevated temperatures in the Earth's crust. In order to establish the diffusion behaviour of He in apatite, step-wise heating experiments have been performed on fragments of Durango fluorapatite [*Zeitler et al.*, 1987; *Lippolt et al.*, 1994; *Wolf et al.*, 1996; *Warnock et al.*, 1997; *Farley*, 2000; *Shuster and Farley*, 2003]. In the simplest case, the radiogenic daughter product would be lost by volume diffusion involving a single, thermally activated process. Under such conditions the temperature dependence of diffusivity is characterised by the Arrhenius relationship:

$$\frac{D}{a^2} = \left(\frac{D_0}{a^2}\right) \cdot e^{\frac{-E_a}{RT}} \tag{2.11}$$

where D is the diffusivity, D_0 is the diffusivity at infinite temperature, E_a is the activation energy, R is the gas constant, T is the temperature in Kelvin and a is the diffusion domain radius [*Fechtig and Kalbitzer*, 1966]. If this relation is obeyed, then measurements of $\ln(D/a^2)$ as a function of reciprocal temperature $(1/T)$ will plot on a straight line with intercept $\ln(D_0/a^2)$ and slope $-E_a/R$ [e.g. *Farley*, 2000;

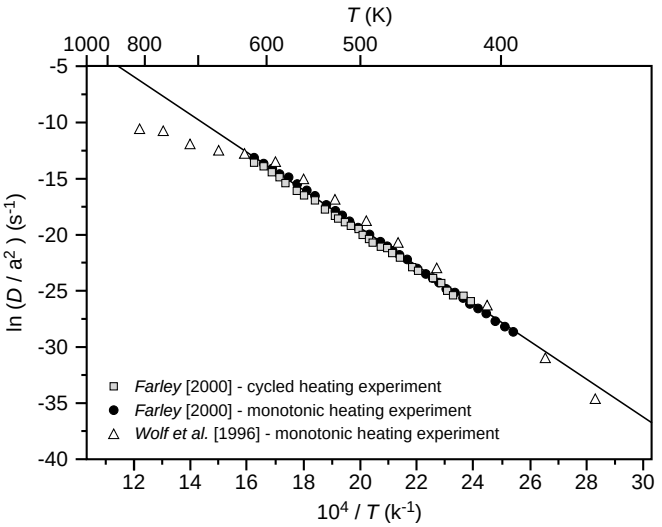

Figure 2.7: Results of step-heating experiments on He extraction from Durango apatite showing measured $D(T)/a^2$ as a function of reciprocal temperature [after *Farley*, 2000]. The data show good Arrhenius behaviour for temperatures $\leq$600 K.

2002]. Laboratory experiments indicated such Arrhenius behaviour, at least at temperatures <300°C (Figure 2.7) [*Farley*, 2000]. From these two quantities the closure temperature T_c can be computed [*Dodson*, 1973], or, more generally, ages can be calculated numerically along arbitrary t-T paths.

Above 300°C the Arrhenius plot is curved. The origin and significance of this curvature has been explored, but remains poorly understood. It has been related to structural or chemical transformations of the crystal or the result of multiple diffusion sites within the apatite [e.g. *Wolf et al.*, 1996], it may be a result of defect annealing in apatite at these temperatures, as fission tracks in apatite also anneal rapidly over this temperature range in the laboratory [*Farley*, 2000] or it has been explained as an artefact of the assumed grain geometry, rather than an actual physical transformation of the apatite grain [*Dunai*, 2000]. The curvature is probably not relevant for He diffusion in the natural setting [*Farley*, 2002].

The diffusion experiments showed that the measured quantity D/a^2 also varies with grain size, such that larger crystals retain a larger fraction of radiogenic He. This suggests that the diffusion domain for He in Durango apatite is the grain itself [*Lippolt et al.*, 1994; *Wolf et al.*, 1996; *Warnock et al.*, 1997; *Farley*, 2000]. From equation (2.11) it then follows that the closure temperature varies with grain size (Figure 2.8) [*Farley*, 2000; *Reiners and Farley*, 2001]. He diffusion from Durango apatite is crystallographic isotropic and thus the relevant dimension for diffusion is the shortest pathway for He loss (i.e. the prism radius) [*Farley*, 2002]. Fractured grains should therefore be avoided, since fractures provide rapid diffusion pathways and will thus change the effective diffusion domain (they effectively reduce "grain-size"). *Reiners and Farley* [2001] have presented AHe age data that support such grain size effects on AHe ages in more typical apatites. *Meesters and Dunai* [2002a] noted that the shape of the diffusion domain is also impor-

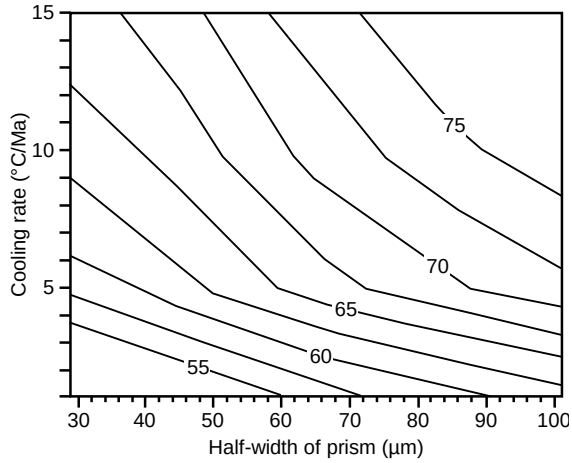

Figure 2.8: Helium closure temperature (T_c) as a function of grain-size and cooling rate, calculated assuming an activation energy of 33 kcal/mol, $D_0 = 50$ cm^2/sec, a spherical geometry and including the effects of α-ejection of He diffusion [after *Farley*, 2002; *Foeken*, 2004].

tant for He diffusion characteristics, especially for apatite grains that have spent significant time close to T_c. This is related to the different surface to volume (S/V) ratios for spherical, rectangular or cylindrical geometries at a given smallest dimension. For geometries having similar S/V ratios these effects are small [*Meesters and Dunai*, 2002b].

From initial diffusion experiments, a closure temperature of 75 ± 5°C was derived for the AHe system (assuming a cooling rate of 10°C/Ma) [*Wolf et al.*, 1996]. In addition, modelling of He production and diffusion in apatites without initial He showed that AHe ages differ with temperature (i.e. depth) for different isothermal holding times (e.g. apatites held isothermally at 75°C for 1 and 10 Ma would yield AHe ages of ∼0.5 and ∼2 Ma, respectively) [*Wolf et al.*, 1998]. Assuming no initial ^{4}He in the apatite crystal, *Wolf et al.* [1998] showed that AHe ages decrease rapidly over a fairly narrow increasing temperature range. In analogy with AFT thermochronology, they named the temperature domain where 5 to 95% of the ^{4}He is retained in the crystal, the Helium Partial Retention Zone (HePRZ). The HePRZ extends from about ∼40°C to ∼85°C for apatite [*Wolf et al.*, 1998] (Figure 2.5). At temperatures >85°C, He is typically lost from the system by rapid diffusion. At temperatures ∼40°C, diffusion becomes slow enough so that He is quantitatively retained in apatite and starts to accumulate [*Wolf et al.*, 1998]. Although the AHe system is described as an open system, i.e. 4He is never 100% retained, variations of ambient temperatures seem to have no marked effect on AHe ages [*Wolf et al.*, 1998].

Several studies attempted to verify the expected diffusion behaviour in natural settings [e.g. *Warnock et al.*, 1997; *Wolf et al.*, 1997; *House et al.*, 1999; *Stockli et al.*, 2000]. Analysis of samples from deep boreholes in which temperature is known as a function of depth confirmed a decrease of AHe ages with increasing depth, but demonstrated that a clear HePRZ is not always present [*House et al.*, 1999].

Studies on rapidly exhumed crustal blocks showed that the HePRZ is apparent in natural settings [*Wolf et al.*, 1997; *Stockli et al.*, 2000]. Comparisons of AHe and AFT ages have confirmed the range of relative temperature sensitivity on geological timescales [*Warnock et al.*, 1997; *House et al.*, 1999; *Farley*, 2000].

Recent developments in AHe thermochronology have shown that various other physical parameters affect He diffusivity in apatite (e.g. presence of inclusions, U and Th zonation, and α-radiation damage). Inclusions in apatites may modify the diffusion behaviour because of the potential difference between the closure temperatures for the host mineral and the inclusion [*Farley*, 2002; *Vermeesch et al.*, 2007]. The effects of mineral inclusions on helium diffusion were modelled by *Vermeesch et al.* [2007]. Their results indicate that, depending on the spatial distribution of the inclusions and their relative α-emitting activity, mineral inclusions might have a non-trivial but minor effect on the closure temperature (<5°C) and could thus induce scatter in the apparent ages for slowly cooled rocks [*Vermeesch et al.*, 2007].

U and Th zonation also affects He diffusion, due to the interference between α-ejection and diffusion [*Meesters and Dunai*, 2002b]. Where the thermal history of samples involves lengthy residence in the HePRZ, the effect of α-ejection on He diffusion can result in ages that are 10–20% older compared to ages without α-ejection. This effect results from the fact that loss by α-emission and the loss by He diffusion should not be considered as independent processes: ejection of α-particles causes the outer parts to become more depleted in radiogenic He than the inner parts, and, hence, it diminishes the effect of diffusive loss since diffusive loss also pertains primarily to the He in the outer parts [*Meesters and Dunai*, 2002b].

Furthermore, α-radiation damage has been demonstrated to affect He retentivity in apatite [*Farley*, 2000; *Crowley et al.*, 2002; *Green and Duddy*, 2006; *Green et al.*, 2006; *Shuster et al.*, 2006; *Flowers et al.*, 2007; 2009; *Shuster and Farley*, 2009]. Increased He retentivity due to the accumulation of radiation damage demonstrably results in a significant increase in effective closure temperature (up to 15°C) over long radiation damage accumulation times, as "traps" are being formed that impede He diffusion [*Shuster et al.*, 2006; *Flowers et al.*, 2007]. This relationship is readily observable in the positive correlation of AHe ages with ^{4}He concentration and effective uranium concentration eU (where $eU = \mathrm{U} + 0.235 \times \mathrm{Th}$) [*Shuster et al.*, 2006; *Flowers et al.*, 2007]. The annealing kinetics of radiation damage in apatite are not yet fully understood, but it seems to be a reversible process in which exposing samples to increasing levels of radiation causes the closure temperature to increase, whereas thermal annealing above certain temperatures (>290°C) causes it to decrease [*Shuster and Farley*, 2009]. The effects of radiation damage are most pronounced in old samples with eU concentrations above ~10 ppm and with complex and slow cooling histories [e.g. *Green et al.*, 2006; *Flowers et al.*, 2007; 2009] (Figure 2.9).

Diffusion studies carried out so far have shown no compositional effect on He retentivity [e.g. *House et al.*, 2002; *Shuster et al.*, 2006], although *Green and Duddy* [2006] emphasized the need for further studies on that topic.

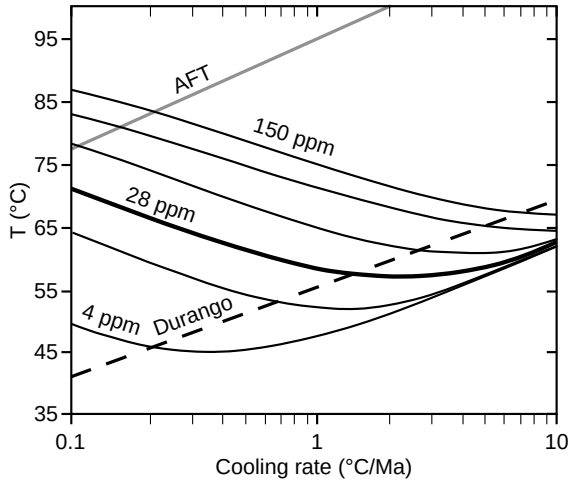

Figure 2.9: Effective closure temperature as a function of cooling rate and eU computed using the radiation damage and annealing model (RDAAM) [after *Flowers et al.*, 2009]. The simulated thermal histories begin at 120°C at different times in the past to yield the reported monotonic cooling rates. Solid black lines are for apatites with different eU values of 150, 100, 60, 15, and 4 ppm from top to bottom. Solid bold line is for typical eU value of 28 ppm. Results for conventional Durango diffusion kinetics (dashed black line) and the AFT system (solid grey line) using the annealing model of *Ketcham et al.* [2007b] are also shown.

2.3.3 Analytical procedures ^{4}He extraction

Samples for AHe analysis were collected from several areas in the Romanian Carpathians (Figure 1.1 and Appendix B): the Apuseni Mountains, (Tables B.1 and B.2), the SE Carpathians (Tables B.3 and B.4), the East Carpathians (Table B.5), the transition zone between the East and SE Carpathians (Table B.6) and the South Carpathians (Table B.7). After mineral separation (see section 2.2.4), inclusion-free apatite grains were carefully handpicked in alcohol under polarized light. Selected grains were photographed and dimensions were measured for α-ejection correction [*Farley et al.*, 1996; *Farley*, 2002]. For all samples, single grain replicates have been analysed (Appendix B). ^{4}He analyses were performed at the Scottish Universities Environmental Research Centre (SUERC) and at the VU University Amsterdam (VUA).

^{4}He measurements at SUERC (Appendix B; Tables B.1, B.3 and B.6) were performed following analytical procedures described by *Foeken et al.* [2006]. Single apatite grains were packed into 1 × 1.5 mm 99.9% pure Pt-foil tubes and loaded into a Cu-planchet, which was placed in the laser chamber. The laser chamber and connecting flexi-tube were degassed at approximately 100°C for about 2 hours to reduce background H, CH_4 and H_2O levels and the system was pumped to $<10^{-9}$ torr by a combination of turbo-molecular and triode ion pumps. Gas was extracted from the apatites by heating the Pt-foil capsules for 1 minute with a diode laser at ∼800°C. Liberated gasses were purified using two liquid nitrogen-cooled traps. ^{4}He abundances were determined by an elec-

tron multiplier in a Hiden HAL-3F Quadrupole mass spectrometer operated in static mode. Absolute ^{4}He concentrations were calculated by peak height comparison against a calibrated standard. The precision of the ^{4}He measurements is determined by the reproducibility of the standard, which is 1.4% (1σ, n = 46) for the duration of this set of experiments (July–August 2006). System blanks were routinely monitored throughout the day (minimum of 2 per day) to assess background ^{4}He levels. ^{4}He blanks yielded $3.3 \times 10^{-12} \pm 2.8 \times 10^{-13}$ ccSTP (n = 5) for RO-samples marked "L" from the SE Carpathians (Table B.3), and $1.8 \times 10^{-12} \pm 3.1 \times 10^{-13}$ ccSTP (n = 19) for the samples from the Apuseni Mountains (Table B.1) and the remaining SE Carpathian samples (Table B.3). Blanks for samples from the transition zone between the East and SE Carpathians (Table B.6) yielded $3.1 \times 10^{-12} \pm 3.2 \times 10^{-13}$ ccSTP (n = 4). Laser heated empty Pt tubes yielded indistinguishable ^{4}He blanks of $2.5 \times 10^{-12} \pm 5.0 \times 10^{-13}$ ccSTP, n = 3). Blank corrections are discussed in full detail in section 2.3.5. Re-extracts were routinely run for each sample, and were all within system background levels.

^{4}He measurements at the VUA (Appendix B; Tables B.2, B.4, B.5 and B.7) were performed following analytical procedures described by *Foeken et al.* [2003]. Single apatite grains were loaded in Inconell cups, which were subsequently placed into a 5 finger extraction unit. The system was pumped overnight by a combination of a turbo pump and two ion getters to about 10^{-8} to 10^{-9} mbarr. Gas was extracted by heating the samples at UHV conditions at 950°C for 35 minutes using an external furnace. Following extraction, gasses were purified using a combination of a SAES getter and a liquid nitrogen trap. ^{4}He abundances were determined by a Hiden HAL-3F/PIC Quadrupole mass spectrometer operated in ion-counting mode and converted from counts per second to ccSTP using an internal ^{4}He standard. The reproducibility of the standard is 1.4% (1σ, n = 18) for November 2004 (Tables B.4 and B.5), 1.1% (1σ, n = 16) for May–June 2005 (Tables B.2 and B.7) and 0.6% (1σ, n = 12) for March 2008 (Table B.2). System background blanks were assessed by heating empty Inconell cups and yielded daily averages ranging from $2.4 \times 10^{-12} \pm 3.4 \times 10^{-13}$ to $9.3 \times 10^{-12} \pm 1.7 \times 10^{-12}$ ccSTP (n = 2 to 5, VUA-measurements 2004) for the SE Carpathian samples (Table B.4), $3.8 \times 10^{-12} \pm 1.9 \times 10^{-13}$ to $1.2 \times 10^{-11} \pm 5.1 \times 10^{-12}$ ccSTP (n = 2 to 4, VUA-measurements 2004) for the East Carpathian samples (Table B.5). System background blanks yielded $7.5 \times 10^{-12} \pm 3.0 \times 10^{-12}$ ccSTP (n = 3, VUA-measurements 2005) for the South Carpathian samples (Table B.7), and $6.3 \times 10^{-12} \pm 2.2 \times 10^{-12}$ ccSTP (n = 5, VUA-measurements 2005) and $4.5 \times 10^{-11} \pm 2.5 \times 10^{-11}$ ccSTP (n = 9, VUA-measurements 2008) for the Apuseni Mountain samples (Table B.2). Re-extracts were routinely run for each sample, and were all within system background levels. Blank corrections are discussed in full detail in section 2.3.5.

2.3.4 Analytical procedures U and Th analysis

U and Th concentrations for all samples were measured by inductively coupled plasma-mass spectrometry (ICP-MS) at the VUA. Laser heated apatites were prepared for U and Th analysis following procedures described by *Balestrieri et al.* [2005]. Following helium extraction, Pt tubes with apatite were transferred

into Teflon beakers. The apatites were dissolved in 5% nitric acid and spiked with a calibrated $^{229}Th/^{233}U$ solution. Subsequently they were placed on a hotplate at 120°C for ∼48 hours. The Pt tubes contain traces of U and Th which could leach out during apatite dissolution. Therefore, prior to packing of the apatite grains and laser He-extraction, empty Pt tubes were leached in 5% nitric acid for 48 hours. Before ICP-MS analyses, the solutions (without Pt tubes) were transferred into 10 ml tubes. Instrument-, full procedure- and Pt blanks were measured to assess U and Th background levels. Full procedure Pt tube blanks for laser heated samples yielded 0.9 ± 0.1 pg and 6.0 ± 0.6 pg (^{238}U and ^{232}Th respectively, n = 2).

Furnace heated apatites were prepared for U and Th analysis following more aggressive dissolution procedures described by *Foeken et al.* [2003] including fluoric acid treatment [see *Vermeesch et al.*, 2007 for the advantages]. HF treatment could not be applied for laser heated apatites as it would dissolve Pt from the tubes and would form interferences in the ICP-MS plasma [*Reiners*, 2005]. Apatites were transferred into Teflon beakers and dissolved in 2 drops of concentrated nitric acid and 5 drops of concentrated fluoric acid, and spiked with the same calibrated $^{229}Th/^{233}U$ solution. Subsequently they were placed on a hotplate at 120°C for ∼48 hours and dried down. Again 2 drops of concentrated nitric acid were added and the solutions were placed on the hotplate at 120°C for ∼24 hours. After drying down the solution, a drop of concentrated nitric acid was added and evaporated. Finally, 0.6 ml of 2N nitric acid was added and left on the hotplate at 100°C for ∼24 hours. After cooling down, 1.2 ml of Milli-Q water was added and the solution was transferred into the ICP-MS tubes. Instrument- and full procedure blanks were measured to assess U and Th background levels. Full procedure blanks for ^{238}U and ^{232}Th yielded 1.4 ± 0.8 pg and 1.8 ± 1.0 pg (n = 4, VUA-2004), 0.9 ± 0.9 pg and 1.1 ± 0.7 pg (n = 4, VUA-2005), and 0.4 ± 0.1 pg and 0.8 ± 0.3 pg (n=5, VUA-2008).

2.3.5 Blank corrections

Because of the sometimes low ^{4}He, ^{232}Th and ^{238}U yield, blank corrections have been applied to all samples (Figure 2.10 and Appendix B). For ^{4}He, the SUERC-measurements yield the lowest blank/sample ratios ranging from <1% for samples with a ^{4}He content of 1.6×10^{-10} ccSTP, to ∼50% for samples with a ^{4}He content of 1.8×10^{-12} ccSTP (diamonds in Figure 2.10a). For the same amounts of ^{4}He, the VUA-measurements 2004 and 2005 yield somewhat higher blank/sample ratios of <5% and ∼60%, respectively (circles and squares in Figure 2.10a). This difference can be explained by the overall lower background ^{4}He-levels inherent to laser heating (e.g. more samples can be loaded at once, shorter extraction and cleaning time). The VUA-measurements 2008 show much higher ^{4}He-blank/sample ratios ranging from 10% up to 82% (triangles in Figure 2.10a). For ^{238}U, there is no significant difference in blank/sample ratios between the VUA- and SUERC-measurements (Figure 2.10b). Samples with U-contents of >0.1 ng required blank corrections of ∼1%, increasing to >10% for samples with <0.01 ng of ^{238}U. For the ^{232}Th, the VUA-measurements samples with Th-contents of >0.1 ng required blank corrections of ∼1–2%, increasing to

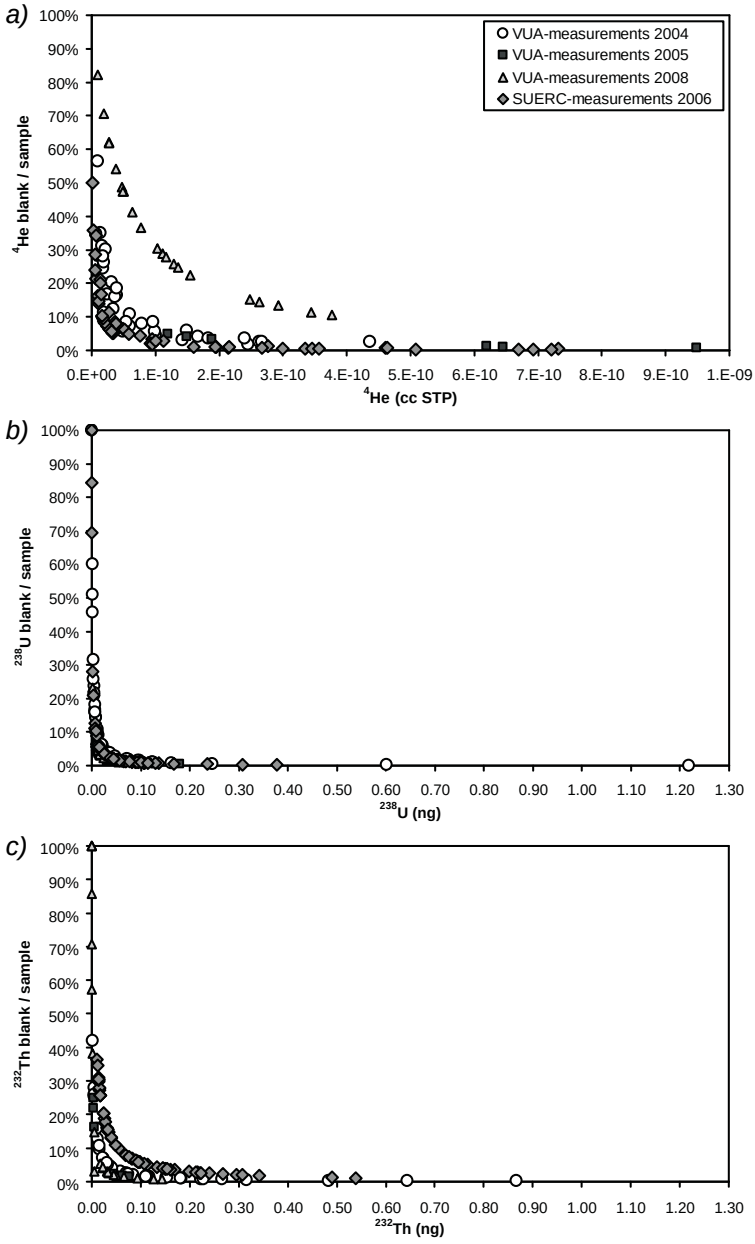

Figure 2.10: Overview of blank/sample ratio versus blank corrected ^{4}He (a), ^{238}U (b) and ^{232}Th (c) content for all samples analysed in this study.

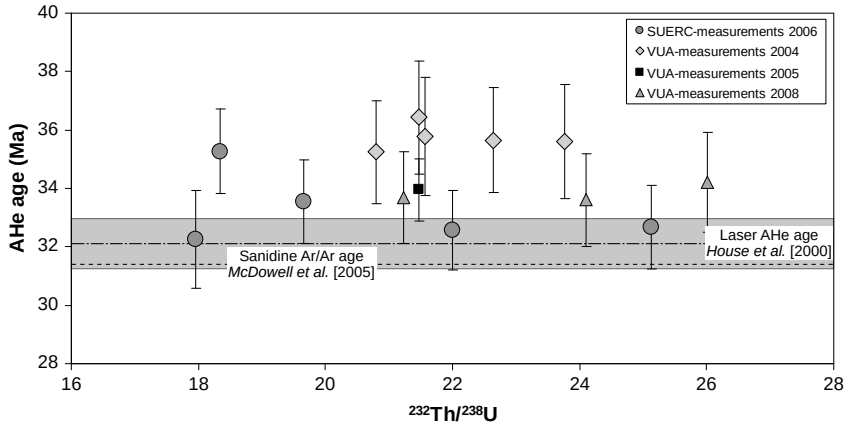

Figure 2.11: Overview of measured Durango standard AHe ages versus Th/U ratio. Solid line with grey band shows mean laser-heated Durango AHe ages of *House et al.* [2000] (32.1 ± 1.7 Ma; 1σ, n = 11); dashed line is single grain sanidine $^{40}Ar/^{39}Ar$ age of *McDowell et al.* [2005] (31.44 ± 0.18 Ma). See text for further discussion.

>15% for samples with <0.01 ng of ^{232}Th (Figure 2.10c). Blank/sample ratios are higher for the SUERC-measurements (Figure 2.10c), which is the result of the high full procedure Pt-tube blank for ^{232}Th. For Th-contents of >0.1 ng, the SUERC-measurements required blank corrections of ∼5–6%, increasing to >30% for samples with <0.01 ng of ^{232}Th (Figure 2.10c). All single grain ages that required ^{4}He, ^{238}U and/or ^{232}Th blank corrections >50% have been excluded from further geological interpretations (Appendix B).

2.3.6 Durango apatite standard

Analytical procedures and age calibrations can be verified by routine analysis of a standard with a known age. The most widely used reference material for AHe thermochronology is the Durango fluorapatite [*Young et al.*, 1969]. The independent reference age of 31.4 ± 0.5 Ma for Durango is provided by K-Ar dating of feldspars [*Green*, 1985, recalculated from *Naeser and Fleischer*, 1975; *McDowell and Keizer*, 1977], refined to 31.44 ± 0.18 Ma by $^{40}Ar/^{39}Ar$ dating of sanidine-anorthoclase crystals [*McDowell et al.*, 2005].

VU Durango fluorapatites (60–180 μm, 1 to 3 fragments) were analysed both by laser (SUERC; Table B.8) and furnace heating (VUA; Table B.8). Blank corrections have been applied in a similar way as for the associated batch of samples. Laser heated Durango apatite ages range between 32.3 ± 1.7 Ma and 35.3 ± 1.5 Ma and yield a mean age of 33.3 Ma with a standard deviation of 1.2 Ma (n = 5; Figure 2.11 and Table B.8). This is in good agreement with the Durango reference age and with previously reported ages for laser heated Durango apatites measured at SUERC [32.6 ± 2.0 Ma, *Foeken et al.*, 2006] and elsewhere [e.g. 32.1 ± 1.7 Ma, *House et al.*, 2000]. Furnace heated Durango ages range between 33.6 ± 1.6 Ma and 36.4 ± 1.9 Ma and yield a slightly older mean age of 34.9 Ma with a standard deviation of 1.1 Ma (n = 9; Figure 2.11 and Table B.9).

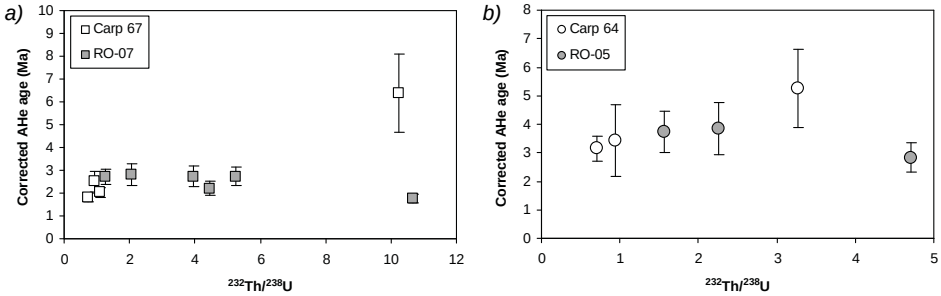

Figure 2.12: Comparison of SUERC and VUA single grain AHe ages for very young samples (<5 Ma) from the same tectonic unit in the SE Carpathians (see Chapter 4 for details on location and geological details). a) Single grain AHe ages versus Th/U ratio for furnace heated sample Carp 67 (open squares; VUA) and laser heated sample RO-07 (grey squares; SUERC). b) Single grain AHe ages versus Th/U ratio for furnace heated sample Carp 64 (open circles) and laser heated sample RO-05 (grey circles).

Within error the mean age overlaps previously reported ages for furnace heated samples measured at the VUA [33 ± 2 Ma, *Juez-Larré*, 2003; 32.1 ± 2.0 Ma, *Foeken et al.*, 2003]. The standard deviation of Durango replicate measurements is 3 to 4%, both for samples analysed at SUERC and the VUA.

2.3.7 AHe age and error calculation

Single grain AHe analytical data are given in Appendix B. The reported 1σ errors on all ages are propagated from analytical uncertainties on U, Th and He determinations and blank corrections, and uncertainties on grain size measurements for F_T-correction. Analytical errors for Durango apatite standards range between 3 and 6% for both VUA and SUERC measurements, which illustrates that the 3 to 4% reproducibility of Durango replicate measurements is defined by the analytical error. Analytical errors for the samples are typically ∼3–6% for SUERC-2006, VUA-2004 and VUA-2005 measurements, increasing to 30% for low-content samples. Analytical errors for the VUA-2008 samples are typically 9–30%, increasing to 100% for low-content samples. The F_T error associated with the uncertainties on the determination of R and L was quantified by repeated measurements of the radius and length on each apatite. These measurements were subsequently averaged to obtain mean R and L values and errors were determined by using an error propagation calculation. Errors on F_T values generally range between 2 and 25%. The analytical error and F_T error were propagated into a total error on the corrected AHe single grain ages. Omitting samples that required blank corrections >50%, they typically range between 5 and 35%.

Some samples yield very young AHe ages (<5 Ma, Tables B.3 and B.4), which is much younger than the ∼32 Ma Durango standard used for inter-laboratory calibration. A comparison of results obtained for similar samples shows that both the SUERC and VUA measurements are able to reproduce these very young ages (Figure 2.12). Samples Carp 67 (furnace-heated) and RO-07 (laser-heated) are both from the same tectonic unit separated by a distance of ∼1–2 km (see 4 for

location and geological details) and yield very similar results (Figure 2.12a). The same applies to Carp 64 and RO-05 (Figure 2.12b), illustrating that both laser- and furnace heated data from two different laboratories yield reproducible young ∼2–4 Ma AHe ages.

For each sample the average and error weighted average of single grain ages has been calculated (Appendix B). The latter has subsequently been used for further geological interpretation (Chapters 3,Chapter 4 and 5). Single grain ages that required blank corrections >50% (e.g. RO-13p2 and p4, Table B.2) and/or that could be identified as obvious outliers with respect to the rest of the single crystal ages from the same sample (e.g. Carp 66p2, Table B.4, also see section 2.3.8) were not taken into account for calculation of an average and error weighted average AHe age.

2.3.8 Intra-sample variations in single crystal ages

Although samples generally yield reproducible results, some samples yield disperse single crystal ages (e.g. RO-09, Table B.3) and/or yield a AHe ages older than their corresponding AFT age (e.g. Carp 97, Table B.1 and Chapter 3). Other samples yield overall reproducible results, but show single grain age dispersions that still exceed the error on the age determination (e.g. RO-02 and RO-06, Table B.3). In general, single crystal ages that are tens to hundreds of million years older than other single crystal ages in a sample can be identified as not belonging to the same population and were excluded from calculation of an error weighted average AHe age. U- or Th-rich inclusions, fluid inclusions or other factors as discussed in sections 2.3.1 and 2.3.2 can be the cause of disperse or anomalously old ages [also see *Fitzgerald et al.*, 2006 for a review of factors].

Although each crystal was subjected to optical inspection, micro-inclusions may be impossible to see under a binocular microscope. During AHe grain selection and inspection of AFT mounts, it was furthermore noted that for some samples it can be very difficult to find apatite grains that are completely free of inclusions (Figure 2.13). Therefore, the effects of micro-inclusions can not be ruled out entirely and might be the cause of some of the anomalously old single crystal ages [e.g. *Lippolt et al.*, 1994; *Farley*, 2002]. Samples which yield obvious outliers that might be related to the presence of inclusions are Carp 66 (Table B.4) and Carp 107 (Table B.5). Some samples did not yield any reproducible results and/or AHe ages much older than AFT ages, which could also be related to the presence of inclusions (e.g. Carp 97 (Table B.1), RO-22, RO-28 (Table B.2), RO-09 (Table B.3), Carp 45 (Table B.4), and Carp 60 (Table B.5)).

For most samples, it can not be clearly distinguished whether factors such as U-Th zonation [*Farley*, 2002; *Meesters and Dunai*, 2002b], variation of crystal size [*Farley*, 2000; *Reiners and Farley*, 2001], He-implantation [*Belton et al.*, 2004; *Spencer et al.*, 2004; *Spiegel et al.*, 2009] or the accumulation of radiation damage [e.g. *Shuster et al.*, 2006; *Flowers et al.*, 2009] play a role. It seems unlikely that effects due to α-ejection correction [*Farley et al.*, 1996; *Farley*, 2002; *Meesters and Dunai*, 2002b; *Dunai*, 2005] can explain some of the anomalously old AHe ages. In order to assess the effects of potential zoning on F_T-correction [*Farley*, 2002; *Meesters and Dunai*, 2002b], the distribution of U was assessed by a first-order

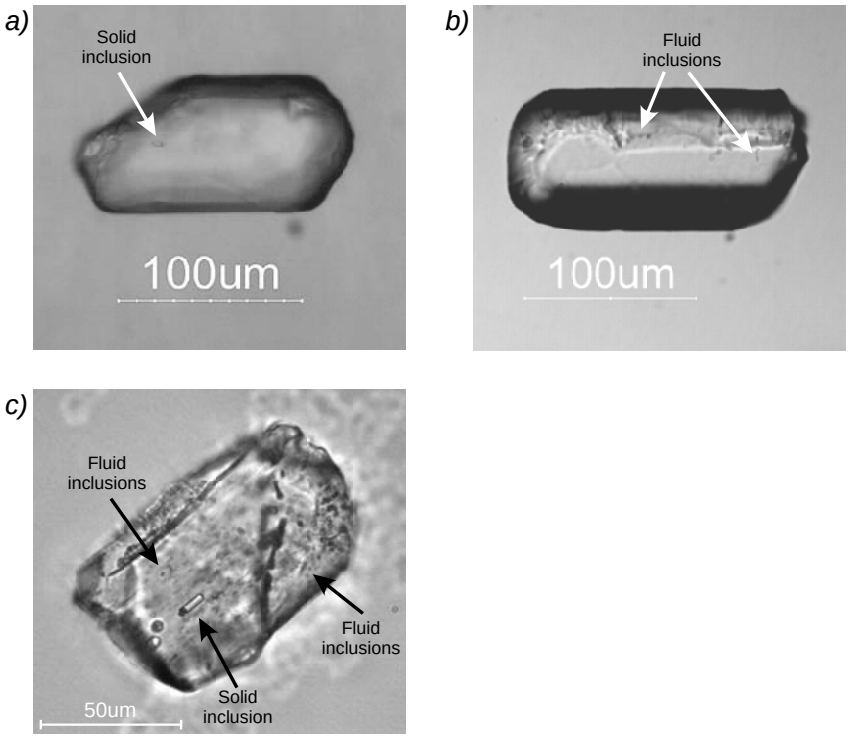

Figure 2.13: Photographs of apatite crystals with solid and/or fluid inclusions. a) Photograph of an apatite crystal with a solid inclusion (Sample RO-04). These are generally large enough to be detected during AHe grain selection (the one shown is $\sim$5 μm). b) Photograph of an apatite crystal with small fluid inclusions (Sample Carp 97). These are generally more difficult to detect during AHe grain selection. c) Photograph of an apatite crystal etched for AFT analysis (sample RO-22). Solid and fluid inclusions are present throughout the apatite grain. The presence of undetected fluid inclusions could play a role in the age dispersion and anomalously old AHe ages that were obtained for this sample.

inspection of AFT mounts and mica detectors, but potential zoning can not be ruled out, because U-contents and thus fission track densities were generally low (see Appendix A). Furthermore, by neglecting the effects of the interplay between α-ejection and He diffusion [*Meesters and Dunai*, 2002b; *Dunai*, 2005], even a severe F_T-overcorrection of $\sim$20% would still be unable to explain the anomalously old AHe ages, particularly in the granitic and volcanic samples (e.g. Carp 97, RO-22 and RO-28, Tables B.1 and B.2).

In the case of crystal size variation, some samples show a positive correlation between AHe age and grain radius (e.g. RO-02, RO-06, RO-11, and Carp 100; Figure 2.14a), whereas other samples do not show this correlation (e.g. Carp 67, Carp 66, Carp 64, RO-07 and RO-09, Figures 2.14b and c). Age dispersion as a result of grain size might explain AHe results for sample RO-11, which has a very large grain-size range (Figure 2.14a).

One sample with a significant age dispersion (RO-09, Table B.3), shows a

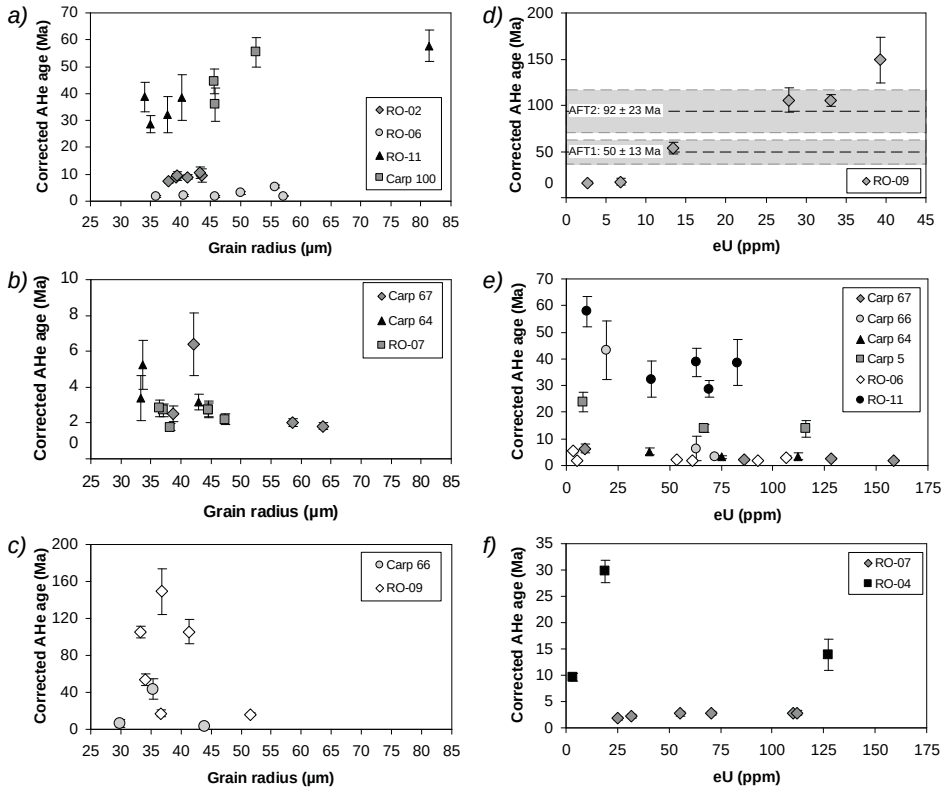

Figure 2.14: Plots illustrating the intra-sample variations of AHe single grain ages. (a), (b) and (c) show grain radius versus AHe single grain age and (d), (e) and (f) of eU concentration versus AHe single grain age.

strong positive correlation between eU and AHe age and some of the single-grain measurements even seem to reproduce for similar eU concentrations (Figure 2.14d). Furthermore, some single grain ages overlap AFT age populations obtained for this sample (Figure 2.14d and Table B.2). Thus it is possible that the AHe age dispersion for this sample might be related to radiation damage. Although most other samples in this study clearly yield young AHe ages (<100 Ma) and their cooling histories are fairly simple (similar AFT and AHe ages), the unusually high eU concentration and significant intra-sample eU variability between crystals for some samples (e.g. RO-06, RO-11, Carp 67, Carp 66, Carp 64 and Carp 5, Tables B.3, B.4 and B.5) invokes speculation that radiation damage arguments might apply and could partly contribute to dispersion of AHe ages. Plots of eU concentration versus single-crystal AHe ages for some of these samples, however, show that crystals with the lowest eU concentrations yield the oldest AHe ages (Carp 67, Carp 66, Carp 64, Carp 5, RO-06, RO-11; Figure 2.14e), which is exactly the opposite as predicted by models assuming the effect of radiation damage. Other samples with similar differences in eU and similar AHe ages do not show any correlation between eU and AHe single grain age (RO-04

and RO-07; Figure 2.14f). Thus the effects of radiation damage can not be clearly identified.

The significant intra-sample variation of eU concentration for this specific group of samples (e.g. <10 ppm for Carp 67p4 and >150ppm for Carp 67p1, Table B.4), does make some of these low eU crystals susceptible to possible He-implantation [e.g. *Belton et al.*, 2004; *Spencer et al.*, 2004; *Spiegel et al.*, 2009], where the high eU apatite crystals could be the source of He-implantation into low eU apatite crystals. Samples RO-22 and RO-28 also have extremely low eU concentrations (<5 ppm) and yield AHe ages much older than the AFT ages (Tables B.1 and B.2), which might be an effect of He-implantation. Carp 97 yields single grain AHe ages that are fairly reproducible (although with large errors), but are much older than AFT ages (Table B.1 and Chapter 3). This sample is a granite with single crystal eU concentrations of 12–20 ppm, which makes them susceptible to potential He-implantation from U-Th rich minerals. Granites are known to contain U-Th rich minerals such as Fe-oxides, titanite and epidote [*Spencer et al.*, 2004].

2.4 Deriving thermal histories and exhumation/denudation estimates from AFT and AHe data

For rapidly monotonously cooled samples, AFT and AHe ages reflect the time at which the rocks passed through the closure temperature, i.e. they constrain a geological event. For more complicated t-T histories, AFT and AHe ages represent apparent ages and modelling of potential t-T paths is required [e.g. *Green et al.*, 1989; *Wolf et al.*, 1998]. This can be done by forward and/or inverse thermal modelling, i.e. by predicting thermochronological results from a specified t-T path or by obtaining potential t-T paths from measured thermochronology data, respectively. This requires characterisation of the thermal behaviour of the thermochronological system, in this case AFT annealing and AHe diffusion.

2.4.1 AFT annealing models

In order to obtain thermal histories from fission track data, the rates at which track lengths are reduced must be estimated. The general method is to use empirical equations calibrated via laboratory experiments. Several empirical [*Laslett et al.*, 1987; *Crowley et al.*, 1991; *Laslett and Galbraith*, 1996; *Ketcham et al.*, 1999; 2007b; *Guedes et al.*, 2007] and semi-empirical [*Carlson*, 1990; *Guedes et al.*, 2006] annealing models have been proposed. The annealing equations are such that points of equal reduced track length ($r = l/l_0$, where l is the measured track length and l_0 is the initial track length) lie on straight or curved lines that are either parallel or meet in a single (fanning) point in Arrhenius space. Although the fits of the different annealing models to the laboratory data are nearly identical, the model predictions deviate significantly once extrapolated over geological timescales [*Ketcham et al.*, 1999] (Figure 2.15). Thus, the extrapolation of the annealing equations to predict temperatures on geological time scales and the calibration against geological data remains a subject of further research for

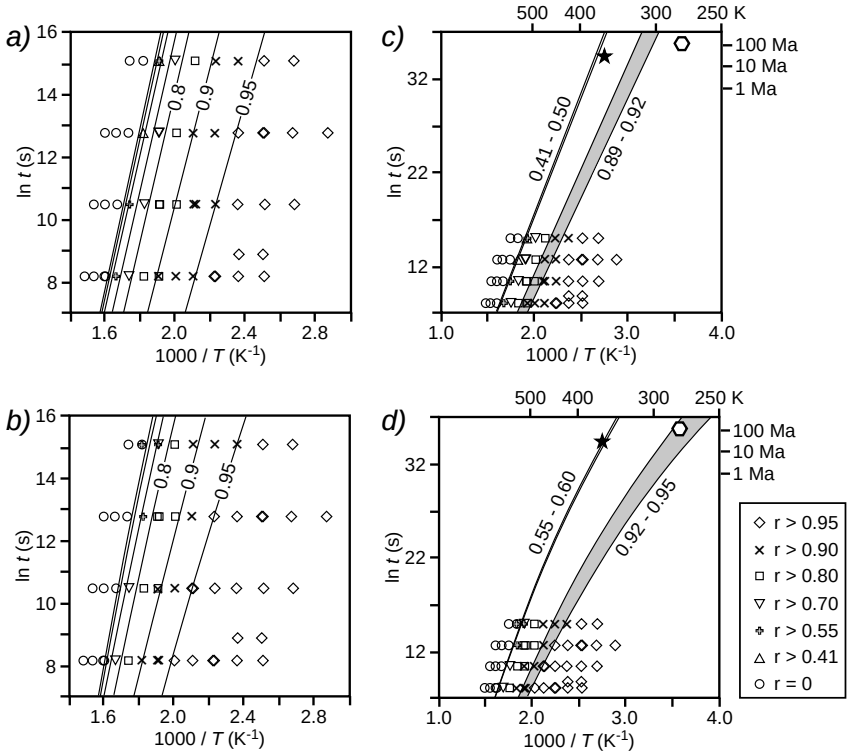

Figure 2.15: Example of fission-track annealing data for apatite and extrapolation to geological time scales [after *Ketcham et al.*, 1999; *Braun et al.*, 2006]. a) and b) show the laboratory annealing data of *Carlson et al.* [1999] for end-member fluorapatite. The relative track-length reduction (r) in different experiments is plotted as a function of ln t and $1/T$. Lines of equal track-length r are plotted for the fanning Arrhenius model (a) and fanning curvilinear model fits of *Ketcham et al.* [1999]. c) and d) show a comparison between model predictions and the two geological benchmarks of *Ketcham et al.* [1999]: the black star indicates the high-temperature benchmark from the Otway Basin [*Gleadow and Duddy*, 1981] and the open hexagon indicates the low-temperature benchmark from the East Mariana Basin [*Vrolijk et al.*, 1992]. Shaded lines indicate the t-T conditions predicted for the amount of r recorded by these samples. The difference in r-values between plots (c) and (d) stems from the fact that in the first plot the raw track-length data are plotted whereas in the latter these are projected to the c-axis.

improving the reliability of thermal history inversion [e.g. *Ketcham et al.*, 1999; 2007b; *Guedes et al.*, 2008].

The predictions of the most commonly used annealing models were evaluated by *Ketcham et al.* [1999] against a high- and low-temperature benchmark, respectively provided by AFT temperature data from drill cores from the Otway Basin [*Gleadow and Duddy*, 1981; *Green et al.*, 1985; 1989; *Green*, 1995] and AFT track length data from seafloor sediments from the East Mariana Basin [*Vrolijk et al.*, 1992]. The calibration showed that the widely used fanning Arrhenius model of *Laslett et al.* [1987] based on Durango apatite data of *Green et*

al. [1986] agrees well with the high-temperature benchmark for apatites of similar Cl-content [*Green et al.*, 1989; *Ketcham et al.*, 1999]. However, the *Laslett et al.* [1987] model predicts too long mean track lengths for the low-temperature benchmark and thus underestimates the length reduction at low temperatures on geological timescales [*Ketcham et al.*, 1999; *Kohn et al.*, 2002]. This may lead to spurious late cooling episodes when t-T histories are fit to data from unknowns [also known as the "Late Neogene cooling artefact"; *Ketcham et al.*, 1999]. On the other hand, the *Crowley et al.* [1991] fanning Arrhenius model based on F-apatite matches the low-temperature benchmark well, but predicts down-hole fading temperatures that are too high for the high-temperature benchmark [*Ketcham et al.*, 1999]. The improved statistical treatment of *Laslett and Galbraith* [1996] considerably lowers the too high temperatures based on the F-apatite measurements of *Crowley et al.* [1991], but increases the predicted length for the low-temperature benchmark.

Ketcham et al. [1999] subsequently suggested a fanning curvilinear model based on c-axis projected lengths [*Donelick et al.*, 1999] of the *Carlson et al.* [1999] data set that is in better agreement with the available geological benchmarks (Figure 2.15). In this multi-kinetic annealing model, the actual track length shortening for any apatite with a specific resistance to annealing is related to that of the most resistant apatite. The fission track annealing properties among analysed natural apatite grains can be assessed by the commonly used kinetic parameters D_{par}, Cl-, and OH-content. Correcting for the angle between the fission track and the crystallographic c-axis will compensate for the difference in annealing behaviour for tracks parallel and perpendicular to the c-axis and the related observer bias [e.g. *Donelick et al.*, 1999; *Ketcham et al.*, 1999; 2009; *Barbarand et al.*, 2003a; *Ketcham*, 2005a]. The *Ketcham et al.* [2007b] model provides an improved annealing model that matches both the *Carlson et al.* [1999] data set and the extensive laboratory annealing data set acquired by *Barbarand et al.* [2003b].

2.4.2 AHe diffusion models

Based on laboratory experiments, several He-diffusion models have been derived [*Wolf et al.*, 1996; *Farley*, 2000; *Shuster et al.*, 2006; *Flowers et al.*, 2009]. *Wolf et al.* [1996] noted a variation in activation energy (E_a) of 30–39 kcal/mol in the apatite samples they studied. It was, however, unclear whether this variation was real or due to the analytical error [*Farley*, 2000]. Diffusion experiments by *Farley* [2000] were conducted on Durango apatite and showed that He-diffusion varies with grain size but provided no compelling evidence that other factors, such as chemical composition, were important. The *Farley* [2000] estimates on E_a (33.0 $\pm$ 0.5 kcal/mol) and the frequency factor, suggested a He closure temperature of $\sim$70°C for an apatite of 70 μm radius assuming a cooling rate of 10°C/Ma. These diffusion kinetics of Durango apatite have been widely used to interpret AHe data, i.e., that the AHe age represents time since the sample cooled through a closure temperature of $\sim$70°C.

Shuster et al. [2006] started to explore how diffusivity varies for apatite samples from many localities. As previously argued by *Lippolt et al.* [1994], they found a

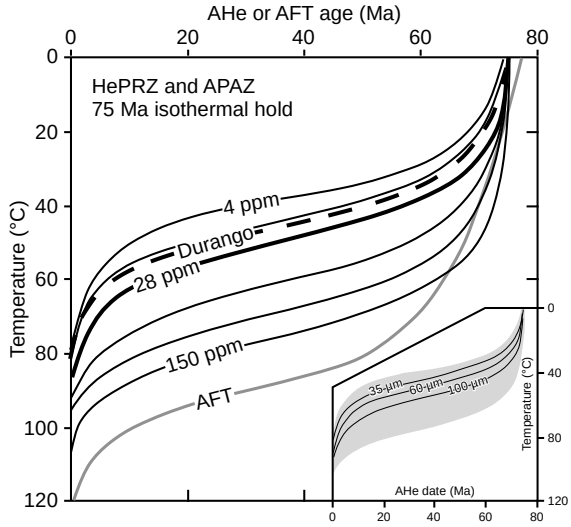

Figure 2.16: The helium partial retention zone (HePRZ) computed for apatites characterized by a range of eU concentrations using the RDAAM following 75 Ma of isothermal holding [after *Flowers et al.*, 2009]. Solid lines are for apatites with eU values of 4, 15, 60, 100, 150 ppm from top to bottom. Solid bold line is for apatite with typical 28 ppm eU value. The HePRZ computed using conventional Durango diffusion kinetics (bold dashed black line), and the APAZ computed using *Ketcham et al.* [2007b] apatite annealing kinetics (grey solid line) are depicted for comparison. The inset depicts the HePRZ for apatites characterized by radii varying from 35 to 100 μm and uniform 28 ppm eU (solid lines), and the variation in HePRZ predicted for eU from 4 to 150 ppm and uniform radius of 60 μm (grey shaded field).

significantly larger variance in closure temperature from 44 ± 4°C to 116 ± 18°C than previously recognised for He in apatite [*Wolf et al.*, 1996; *Warnock et al.*, 1997; *Farley*, 2000; *Shuster and Farley*, 2005]. *Shuster et al.* [2006] showed that the variance in closure temperature is not a simple function of either E_a or D_0, but some combination. The *Shuster et al.* [2006] data did not suggest a clear correlation between apatite composition (e.g. F/Cl ratio) and closure temperature as observed in AFT annealing [*Gleadow and Duddy*, 1981; *Green et al.*, 1986; *Donelick*, 1991; *O'Sullivan and Parrish*, 1995]. However, a significant linear correlation between closure temperature and ^{4}He concentration suggested that exposure to intense natural radiation flux caused the samples to become more He-retentive [*Shuster et al.*, 2006]. Based on these observations, *Shuster et al.* [2006] developed the He-based trapping model (HeTM). This He-diffusion model predicts that the effective closure temperature of apatite varies with cooling rate and effective U-concentration (eU), in such a way that AHe ages of monotonically cooled apatites are associated with effective closure temperatures that bracket the Durango model, but may differ from that model by up to ∼15°C. Furthermore, it predicts that the depth of the HePRZ will depend on accumulation time and eU, and that samples subjected to reheating after accumulation of substantial radiation damage will be more retentive.

The effects of radiation damage on He diffusion were further explored by *Flowers et al.* [2007], *Shuster and Farley* [2009] and *Flowers et al.* [2009]. *Shuster and Farley* [2009] confirmed that the addition of radiation damage increases an apatite's closure temperature, but also showed that thermal annealing of the damage at temperatures >290°C (>1h) reverses this effect. *Shuster and Farley* [2009] and *Flowers et al.* [2009] mentioned that the correlation between He closure temperature and effective fission track density may suggest that fission track damage controls He-diffusion. However, an alternative and equal valid explanation provided by *Flowers et al.* [2009], is that α-decay damage from parent recoil and/or the α-particle itself anneals with the same kinetics as fission damage. Furthermore, they argue that α-decay rather than fission is the major factor controlling He-diffusion in apatite. Based on further experiments on the relationship between He-retention and the AFT method, two proxies for radiation damage were suggested. One model suggests correlation between FT length reduction with a decrease in He-retention [*Shuster and Farley*, 2009]. However, since the track lengths alone do not accurately document volume fraction of radiation damage it was argued that this is not a robust proxy [*Flowers et al.*, 2009]. The other model suggests the use of effective spontaneous fission track density [*Flowers et al.*, 2009]. This was incorporated into the radiation damage accumulation and annealing model (RDAAM) [*Flowers et al.*, 2009]. Use of the RDAAM seems particularly important for accurate interpretation of AHe data for apatite samples that experienced moderate to slow monotonic cooling (0.1–1.0°C/Ma, Figure 2.9), prolonged residence in the HePRZ (Figure 2.16), or prolonged residence at temperatures appropriate for radiation damage accumulation followed by reheating and partial He-loss [*Flowers et al.*, 2009].

2.4.3 Thermal modelling

Thermal modelling of samples analysed in this study was carried out with the HeFTy program (version 1.3c) [*Ketcham*, 2005b], using both AFT age- and length and AHe data. Samples with non-reset AFT ages and/or multiple age populations were modelled using the AHe data only. The present-day surface temperature was set to 10 ± 5°C. Additional model inputs are geological constraints (e.g. stratigraphic or magmatic ages, stratigraphic unconformities and well constrained tectonic phases).

The annealing model of *Ketcham et al.* [1999] was used for modelling of the AFT data using D_{par} as kinetic indicator. Using the *Ketcham et al.* [1999] model requires the use of the etching procedure as outlined by *Carlson et al.* [1999]. *Carlson et al.* [1999] show that the default initial track length (l_0) systematically correlates with certain measurable parameters including D_{par} ($l_0 = 15.63 + 0.283 \times D_{par}$). Although the VU etching procedure differs from the one by *Carlson et al.* [1999], the annealing model of *Ketcham et al.* [1999] was preferred because it allows correcting for track angle using the c-axis projection model of *Donelick et al.* [1999] to increase the consistency of the measurements and to compensate for Cf-irradiation and observer bias [e.g. *Barbarand et al.*, 2003a; *Ketcham*, 2005a; *Ketcham et al.*, 2007a; 2009]. The effect of the different etching methods was calibrated by *Murrell* [2003] and *Murrell et al.* [2009], who showed that the average

ratio for ${D_{par}}^{VU}/{D_{par}}^{Carlson}$ is 1.255 (where ${D_{par}}^{VU}$ is the etch pit diameter obtained with the VU etching method and ${D_{par}}^{Carlson}$ is the etch pit diameter obtained with the *Carlson et al.* [1999] etching method). For ${D_{par}}^{VU}$ values of 1.2 to 2.3 μm for the Apuseni Mountains (Table A.1 I.1) and 1.0 to 1.6 μm for the SE Carpathians (Table A.2) the difference would produce l_0 values of 0.058 to 0.132 μm greater than the "real" values that would have been obtained using the *Carlson et al.* [1999] etching method. *Carlson et al.* [1999] stated that 0.5 μm variation in l_0 leads to a difference (overestimation) of 10–15°C in predicted temperature of a t-T path. Using the annealing model of *Ketcham et al.* [1999] on this dataset would imply an overestimation of 1.2–4.0°C, which is considered negligible in this study and falls within the errors of the modelling process.

For the AHe data, the *Farley* [2000] Durango He-diffusion model was used. Whereas more recent diffusion models [e.g. *Shuster et al.*, 2006; *Flowers et al.*, 2009] have become available, the *Farley* [2000] diffusion model is justified for these samples as they have young ages (AFT and AHe <100 Ma, Appendices A and B) and appear to have experienced rapid cooling (similar AFT and AHe ages). Furthermore, most samples have eU concentrations below or equal to the typical value of 28 ppm as defined by *Flowers et al.* [2009] and will yield RDAAM closure temperatures (Figure 2.9) and HePRZ depths (Figure 2.16) very similar to the ones calculated using the conventional Durango diffusion model. The few samples from the East and SE Carpathians that did yield exceptionally high eU concentrations (∼100–150 ppm, see section 2.3.8 and Appendix B) are characterised by cooling rates far higher than 10°C/Ma (Chapters 3 and 5) and thus the predictions from the *Flowers et al.* [2009] RDAAM will also be similar to the conventional Durango diffusion kinetics (Figure 2.16). The model precision was set to "best-fit" to produce the corrected age using the α-ejection correction model of *Farley et al.* [1996]. Although a more detailed α-calculation option is provided by *Ketcham* [2009], in which an F_T is calculated for each isotope and applied separately in the age equation, this is not important for samples from this study, since it gives results that are equivalent to the *Farley et al.* [1996] equation for AHe ages <500 Ma [*Ketcham*, 2009].

2.4.4 Conversion of time-temperature histories into exhumation / denudation estimates

In order to assign a geological meaning, AFT and AHe cooling ages and modelled t-T histories are often translated in terms of exhumation by estimating a geothermal gradient. Hereby it is assumed that cooling results from the removal of an overlying rock column by erosion and/or (tectonic) denudation. Positive exhumation means rocks move closer to the Earth's surface (i.e. unroofing), and negative values for exhumation or exhumation rates, mean that rocks move further away from the Earth's surface, i.e. are buried [*England and Molnar*, 1990; *Stüwe and Barr*, 1998]. In the context of orogenic evolution, exhumation may reflect enhanced erosion as a result of tectonically induced uplift (an increase of topographic elevation caused by crustal thickening) or of external forces such as a base-level lowering. The terms rock uplift and surface uplift (or just uplift) represent the vertical motion of rocks and the Earth's surface, respectively, relative

to a fixed reference level (i.e. the geoid or mean sea level) [*England and Molnar*, 1990].

Amounts and rates of cooling were derived from the modelled t-T histories. Regional heat flow data were used to calculate a (paleo)-geothermal gradient to convert cooling into exhumation and denudation estimates. Errors on amounts and rates of cooling, and on the estimated geothermal gradients were propagated into the errors on exhumation and denudation estimates.

For the Apuseni Mountains (Figure 1.1 and Chapter 3), using present-day regional heat-flow values of ∼60 mW/m^2 [*Dövenyi and Horváth*, 1988; *Demetrescu and Andreescu*, 1994] and average thermal conductivities of ∼2–4 W/m/°C, a geothermal gradient of ∼25 ± 10°C/km was calculated. However, extrapolating this present-day geothermal gradient to a paleo-geothermal gradient is not straightforward given the significant Miocene re-heating of the Pannonian lithosphere during the back-arc extension. It is likely that the heat-flow of the Apuseni Mountains was lower during the Cretaceous–Paleogene stages of orogenic growth. Therefore, using a paleo-geothermal gradient estimated from present-day heat-flow values may lead to an underestimation of Cretaceous–Paleogene exhumation.

For the SE Carpathians (Figure 1.1 and Chapter 4), a (paleo)-geothermal gradient of 20 ± 5°C/km is estimated based on present-day surface heat flow values of ∼40–60 mW/m^2, thermal conductivities of 1.7–4.5 W/m/°C, and previously published geothermal gradients [*Veliciu and Visarion*, 1984; *Demetrescu et al.*, 2001; *Andreescu et al.*, 2002; *Demetrescu et al.*, 2007]. This estimate is in agreement with modelling results of the Miocene thermal evolution of the foreland basin [*Demetrescu et al.*, 2007]. Note that by assuming this relatively low geothermal gradient, amounts and rates of exhumation represent maximum estimates. The exception from this calculation is the area close to the Quaternary volcanics of the Perşani Mountains (Chapter 4), where a present-day heat flow of ∼60–90 mW/m^2 is observed. Thus, a geothermal gradient of 35 ± 10°C/km was adopted for late Neogene cooling in the Perşani Mountains (sample RO-10).

For the East and South Carpathians (Figure 1.1 and Chapter 5), regional heat flow data [*Veliciu and Visarion*, 1984; *Demetrescu et al.*, 2007] were used to calculate a (paleo)-geothermal gradient of 20 ± 5°C/Ma for the East Carpathians and 25 ± 10°C/Ma for the South Carpathians.